MICROBIAL-CADDISFLY BIOHERM ASSOCIATION OF THE LOWER CRETACEOUS SHINEKHUDAG FORMATION, MONGOLIA

by

Tsolmon Adiya

A thesis submitted to the faculty of
The University of Utah
in partial fulfillment of the requirements for the degree of

Master of Science

in

Geology

Department of Geology and Geophysics

The University of Utah

August 2017

The University of Utah Graduate School

STATEMENT OF THESIS APPROVAL

The thesis of **Tsolmon Adiya**

has been approved by the following supervisory committee members:

Cari Johnson	, Chair	**04/13/2017** Date Approved
Mark Loewen	, Member	**04/13/2017** Date Approved
Kathleen Allabush	, Member	**04/13/2017** Date Approved

and by **Thure Cerling**, Chair/Dean of

the Department/College/School of **Geology and Geophysics**

and by David B. Kieda, Dean of The Graduate School.

ABSTRACT

Caddisfly larvae construct underwater protective cases using surrounding materials, providing information on environmental conditions in both modern and ancient systems. Microbial bioherms associated with caddisfly cases are found in the Berriassian-Hauterivian (~140-130 Ma) Shinekhudag Formation of Mongolia and provide new insights into aspects of lacustrine paleoecosystems and paleoenvironments. This formation contains the earliest record of plant-armored caddisfly cases and a rare occurrence of microbial-caddisfly association from the Mesozoic. The bioherms are investigated within the context of stratigraphic correlations, depositional environment interpretations, and basin-evolution models of the sedimentary fill. The bioherms form 0.5-2.0 m diameter mound-shaped bodies and are concentrated within a single, oil shale-bound stratigraphic interval. Each bioherm is composed of up to 40% caddisfly cases along with millimeter-scale, laminated stromatolites. Petrographic analyses reveal these bioherms are composed of non-systematic associations of columnar and oncoidal microbialites, constructed around colonies of caddisfly cases. The cases are straight to curved, slightly tapered, tube-shaped, with a progressively increasing length and width trend (7-21 mm by 1.5-2.5 mm). Despite these variations, the case architectures reveal similar construction materials; the armor is dominated by plant fragments, ostracod valves, carbonate rock fragments, and rare mica and feldspar grains. The bioherms contain various allochems including ooids, ostracods, plant fragments, rare gastropods,

feldspar grains bound in micritic matrices, and carbonate dominated cements. The combination of microbial-caddisfly association, plant fragment case armors, and ooids/oncoids indicates a shallow, littoral lake setting. Stratigraphic juxtaposition of nearshore bioherms and the bounding distal oil-shale facies suggests that the bioherms developed in an underfilled lake basin, resulting from rapid lake desiccation. Lake chemistry is believed to have been relatively alkaline, saline to hypersaline, and rich in Ca, Mg, and HCO_3 ions. Through analyzing bioherm characteristics, caddisfly case architecture, carbonate microfacies, and stratigraphic variability, we infer larger-scale processes that controlled basin development during their formation.

I dedicate this thesis to my loving family, husband Bat-Erdene and daughter Enkhbileg.

TABLE OF CONTENTS

LIST OF FIGURES

ACKNOWLEDGEMENTS

I would like to thank all the people who contributed to this research and thesis. First and foremost, I express my sincere gratitude to my advisor, Professor Cari Johnson, for accepting me to work with her, and supervising my research as well as my studies at the University of Utah. I have deeply benefited from her immense knowledge and experience, and I am certainly a better geologist now. I also would like to thank for my supervisory committee members, Dr. Mark Loewen and Dr. Kathleen Allabush, for their encouragements, guidance, and motivation throughout this research.

Also, a very special gratitude goes to my sponsor, the Fulbright Foreign Student Scholarship, for making my higher education possible. My acknowledgment is extended to my fellow students and labmates, particularly to “Team Cari”, and my IBA teammates. Special thanks to Ellen Reat for her great help and insights of academic writing. Finally, my genuine deepest appreciation goes to my family, my husband Bat-Erdene and daughter Enkhbileg, for their constant love and support. This project is more yours than mine.

INTRODUCTION

Fossil insects are well-known in geological records and, in addition to their entomological and paleontological implications, have also been used as paleoenvironmental indicators, particularly in lacustrine systems (Wilson, 1980; 1988; Elias, 1991; Drysdale et al., 2003; Kuzmina et al., 2008). Out of millions of insect taxonomic orders, the caddisflies are distinguished by their adaptive and innovative behavior. Caddisflies are fully aquatic during their larval and pupal stage, when they typically build hard cases to cover their soft bodies, using materials from their immediate surrounding aquatic environment (Ross, 1967). Fossil caddisflies and their cases appear as early as Triassic time, both in aquatic and terrestrial realms, surviving the major Mesozoic to Cenozoic extinction events and aftermaths (Shcherbakov, 2008). The creative construction of hard cases for protection and respiration purposes is critical to caddisflies' survival and adaptation skills (Wiggins, 2004).

Case studies of the Eocene Green River Formation in Wyoming, USA have demonstrated the effectiveness of fossil caddisfly case analysis for sedimentary facies predictions and paleoenvironmental reconstructions (Loewen et al., 1999). Here, thousands of caddisfly cases are found within a thick sequence of microbially-influenced lacustrine carbonates (Buchheim et al., 2012; Seard et al., 2013). Generally, carbonate facies of the lacustrine systems are altered by both biological and depositional processes, and thus these strata contain important insights to the paleoecosystem and

paleoenvironment (Embry and Klovan, 1971; Wright, 2012). In the Green River Formation, the co-existence of fossil caddisfly cases and microbialites was used to infer a depositional model for carbonate bioherm facies (Leggitt et al., 2001; 2002; 2007), because each of these biologic components (caddisfly and microbialite) have environmental preferences and tolerances including light, oxygen, and nutrient availabilities that are fundamentally dependent on wave energy, bathymetry, lake hydrology, and lake chemistry (Burne et al., 1987; Riding, 2000; Bohacs et al., 2007). Additionally, the debris incorporated in the caddisfly larval cases reveal the main compositions of the environment (Leggitt et al., 2007). Therefore, the paleoenvironment interpretations require detailed evaluation of the biologic components' trace, particularly for the caddisfly cases. Fossil records of the caddisflies and their cases date back to the Triassic, and multiple early Cretaceous examples documented from Asia including China, Korea, and Mongolia (Ivanov & Sukatsheva, 2002; Paik, 2005; Shcherbakov, 2008). However, our current knowledge of caddisflies is mainly limited to Eocene and younger examples (e.g., Eocene Green River Formation, Oligocene Indusial Limestone Formation) due to excellent exposures and preservation in these sections (Hugueney, 1990; Botosaneanu et al., 2004; Leggitt et al., 2007).

Here we present a case study from the Early Cretaceous Tsagaansuvarga Basin of Mongolia (Fig. 1). The carbonate bioherm facies, similar to those in the Green River Formation, are found within lacustrine basin fill and provide an excellent opportunity to test the use of fossil caddisfly case analysis for carbonate facies interpretation and paleoenvironmental reconstructions. Using these interpretations from the basin, we reveal overall evolution of the lake basin in response to larger-scale processes. Additionally, we

aim to improve the knowledge base of the underwater behavior and evolution of the caddisfly through investigating their case architecture.

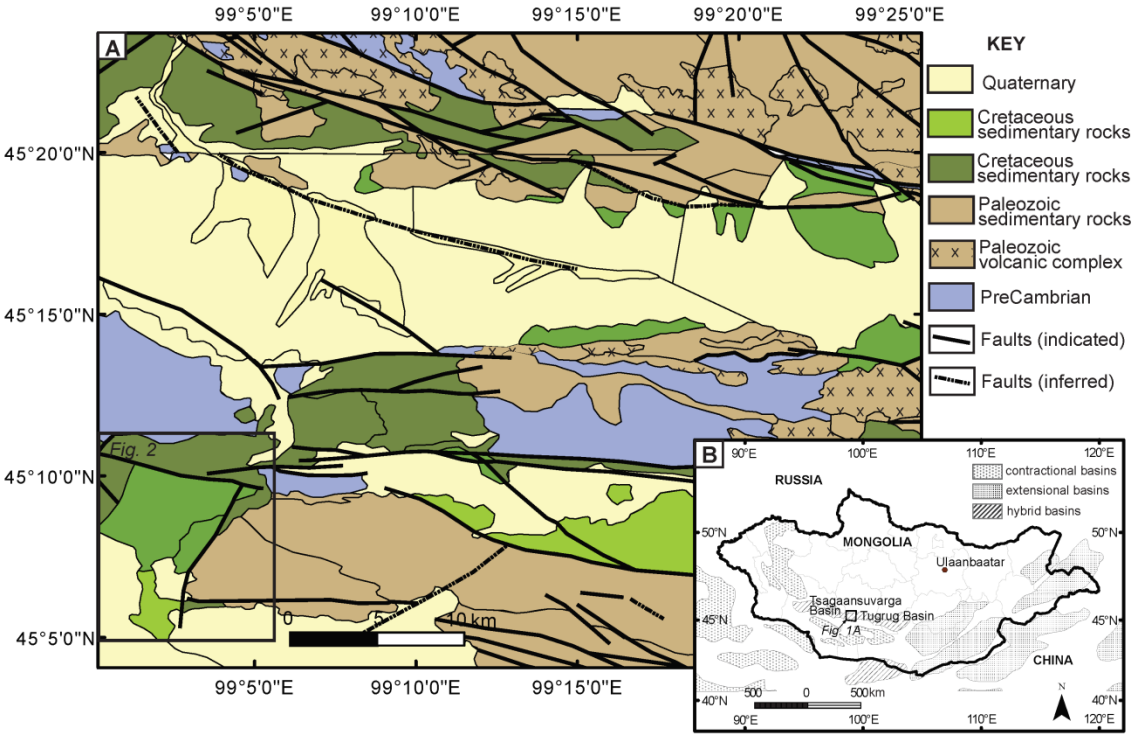

Figure 1. Regional geological map and Mesozoic sedimentary basins of Mongolia. (A) Regional geological map showing major rocks units. The Tsagaansuvarga Basin is located in black boundary (modified after Zabotkin et al., 1988). (B) Mesozoic sedimentary basins of Mongolia (modified after Zabotkin et al., 1988; Johnson et al., 2015). Refer to the keys for map units and symbols

GEOLOGICAL BACKGROUND

The Tsagaansuvarga Basin is part of the broad late Mesozoic sedimentary basin located in southwestern Mongolia (Fig. 1, 2), and interpreted to be a Late Jurassic-Early Cretaceous rift basin (Johnson et al., 2014). This interpretation is based on seismic data showing normal faults with Mesozoic growth strata, the abundance of bimodal volcanics, and regional correlations with well-known Jurassic-Cretaceous rift basins to the southeast in Mongolia and throughout eastern China (Fig. 3; Watson et al., 1987; Graham et al., 2001; 2012; Meng, 2003; Johnson et al., 2004; 2015).

The basement rocks of the basin include Precambrian aged metamorphic and igneous suites of multiple terranes and cratonal blocks, which were accreted during Neoproterozoic to Cambrian time (Badarch et al., 2002; Kelty et al., 2008). These units are overlain by Paleozoic prerift rocks, which are mainly volcanic arc successions (Zabotkin et al., 1988; Ariunchimeg et al., 2011). In the Tsagaansuvarga Basin, these Paleozoic units include Ordovician, Silurian, and Devonian sedimentary strata and volcanic units, as well as Carboniferous and Permian sedimentary rocks and intrusive complexes (Fig. 1).

Upper Jurassic—Lower Cretaceous basin fill includes more than 2 km of exposed volcanic and sedimentary sections, including alluvial fan to fluvial and lacustrine deposits (Zabotkin et al., 1988; Johnson et al., 2014). Mesozoic synrift sedimentation initiated with the Shariliin and Tsagaantsav Formations, which consist of up to 1600 m thick

volcanic units interbedded with thin shallow lacustrine facies (Fig. 3; Horton et al., 2013, Johnson et al., 2014). The volcanic units are mainly bimodal in composition, including both mafic and felsic extrusive flows and their tuffs. These volcanic deposits are overlain by lacustrine facies of the Shinekhudag Formation and its equivalents (Fig. 3). The Shainshand and Bayanshiree Formations unconformably overlie the Shinekhudag Formation and its equivalents, and are mainly composed of alluvial, fluvial clastic sedimentary strata (Fig. 3; Zabotkin et al., 1988; Ariunchimeg et al., 2011).

Most of the modern basin cover is mapped as Paleogene, Neogene, and Quaternary unconsolidated sediments (Fig. 1, 2). The east-west-trending Gobi-Altai active fault system lies along the eastern boundary of the basin. This late Cenozoic feature records sinistral transpression driven by far field deformation driven by the India-Asia collision, as recorded throughout the Gobi-Altai region (e.g., Cunningham, 2005; 2010).

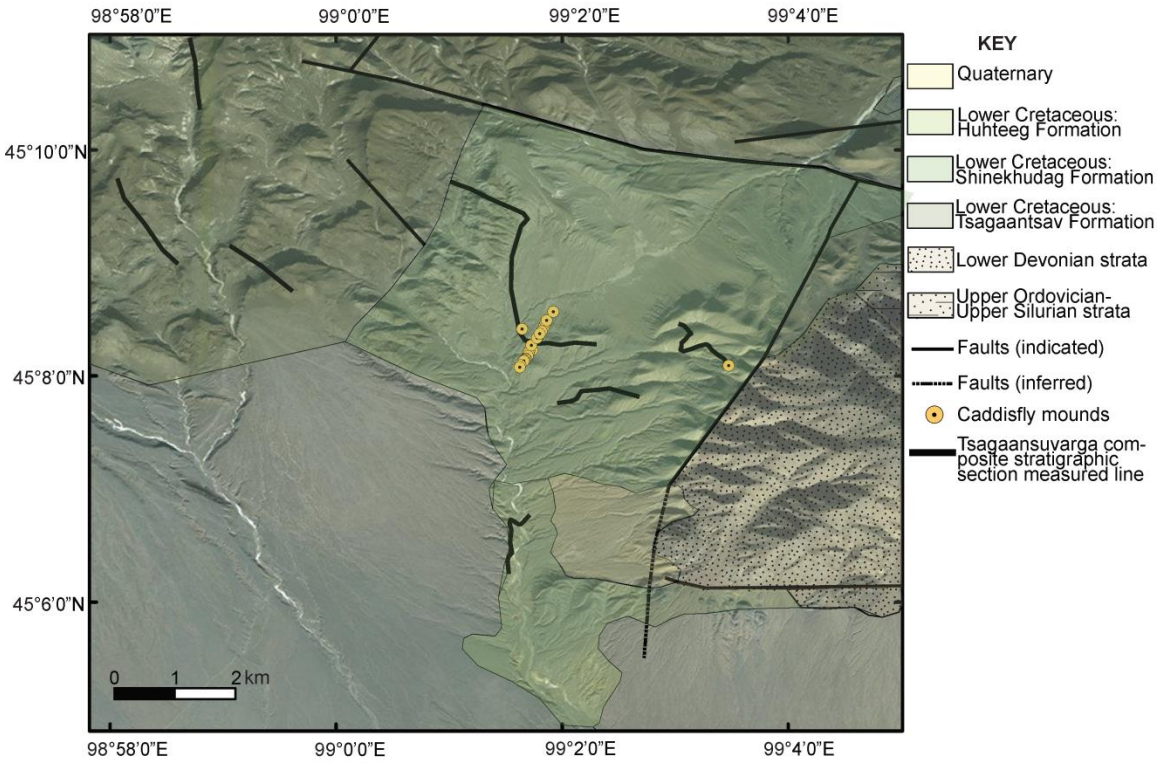

Figure 2. Local geological map overlain on the satellite imagery (modified after Zabotkin et al., 1988). Refer to the keys for map units and symbols.

Figure 3. Regional stratigraphic correlation of Late Mesozoic of Mongolia (modified after Graham et al., 2001; Horton et al., 2013).

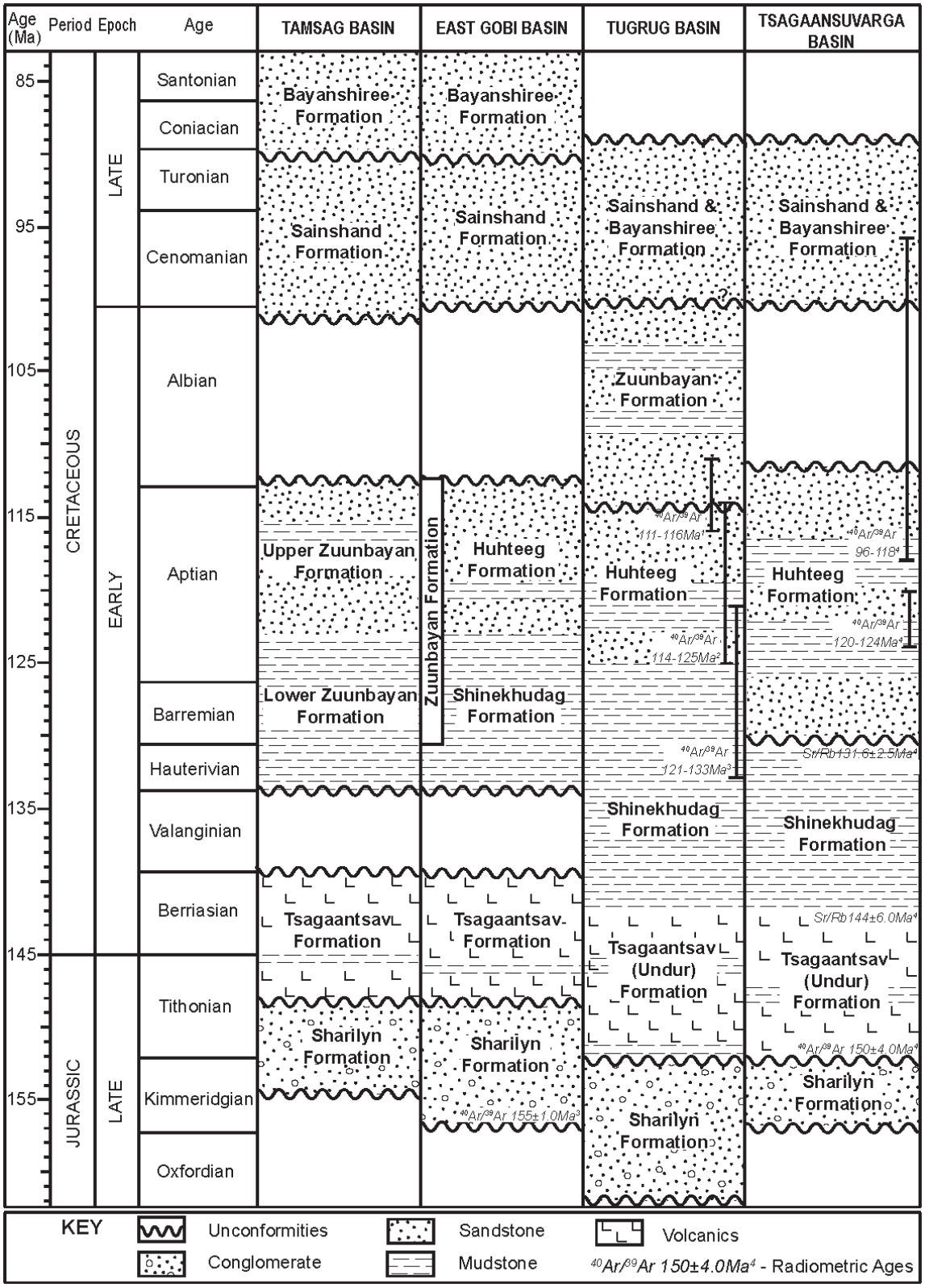
Age (Ma)
Period
Epoch
Age
TAMSAG BASIN
EAST GOBI BASIN
TUGRUG BASIN
TSAGAANSUVARGA BASIN
85
95
105
115
125
135
145
155
CRETACEOUS
JURASSIC
LATE
EARLY
LATE
Santonian
Coniacian
Turonian
Cenomanian
Albian
Aptian
Barremian
Hauterivian
Valanginian
Berriasian
Tithonian
Kimmeridgian
Oxfordian
Bayanshiree Formation
Sainshand Formation
Upper Zuunbayan Formation
Lower Zuunbayan Formation
Zuunbayan Formation
Huhteeg Formation
Shinekhudag Formation
Tsagaantsav Formation
Sharilyn Formation
Sainshand & Bayanshiree Formation
Zuunbayan Formation
Huhteeg Formation
Shinekhudag Formation
Tsagaantsav (Undur) Formation
Sharilyn Formation
40Ar/39Ar 111-116Ma1
40Ar/39Ar 114-125Ma2
40Ar/39Ar 121-133Ma3
40Ar/39Ar 155±1.0Ma3
40Ar/39Ar 96-118Ma4
40Ar/39Ar 120-124Ma4
Sr/Rb131.6±2.5Ma4
Sr/Rb144±6.0Ma4
40Ar/39Ar 150±4.0Ma4
KEY
Unconformities
Conglomerate
Sandstone
Mudstone
Volcanics
40Ar/39Ar 150±4.0Ma4 - Radiometric Ages

MATERIALS AND METHODS

Local field mapping of the Tsagaansuvarga Basin was conducted using a base of regional geological maps and satellite images. A compiled stratigraphic section of 4200 m was measured through the Jurassic-Cretaceous strata, primarily focusing on describing the lithology, grain size, sedimentary structures, and architecture of strata to interpret facies and depositional environments (Fig. 2). Our main focus was on the lower interval of the Shinekhudag Formation (1800 m-2862 m; Fig. 4) of finely laminated mudstone, as this has been previously identified as prospective hydrocarbon source rocks (Johnson et al., 2014). The putative microbial-caddisfly bioherms of primary interest for this study are located in one discrete interval within this section.

A total of 22 hand samples were collected from these bioherms and all were analyzed for hand sample description. Sixteen standard and large format petrographic thin sections were prepared from the hand samples for microscopic analysis. Three of them were partially stained in alizarine red-S dye for identification of carbonate minerals. A combination of Zeiss Axio Imager M2m petrographic scope, Zeiss Zen Blue Professional Software, and ImageJ 1.46r Software permitted qualitative grain and fossil size measurements, counts, and percentage estimation.

Figure 4. Tsagaansuvarga composite stratigraphic section. (A) Entire Tsagaansuvarga basin fill from Upper Jurassic to Lower Cretaceous. (B) Main lacustrine facies of Tsagaansuvarga Basin (lower and upper interval). (C) Close view of microbial-caddisfly bioherm containing lower interval. Refer to the keys for lithologies and sedimentary structures.

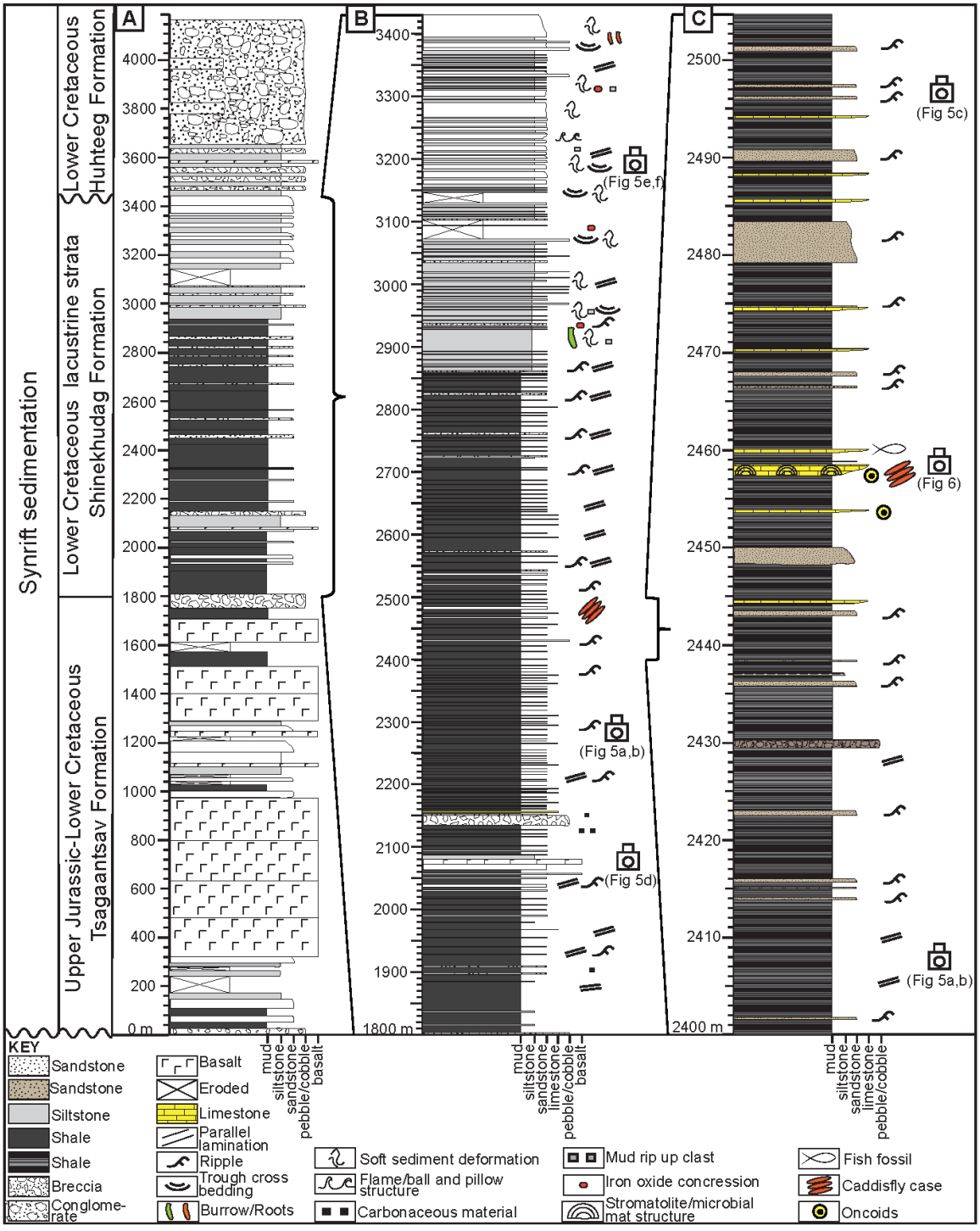
Synrift sedimentation
Lower Cretaceous Huhteeg Formation
Lower Cretaceous lacustrine strata Shinekhudag Formation
Upper Jurassic-Lower Cretaceous Tsagaantsav Formation
A
B
C
4000
3800
3600
3400
3200
3000
2800
2600
2400
2200
2000
1800
1600
1400
1200
1000
800
600
400
200
0 m
3400
3300
3200
3100
3000
2900
2800
2700
2600
2500
2400
2300
2200
2100
2000
1900
1800 m
2500
2490
2480
2470
2460
2450
2440
2430
2420
2410
2400 m
(Fig 5e,f)
(Fig 5a,b)
(Fig 5d)
(Fig 5c)
(Fig 6)
(Fig 5a,b)
mud
siltstone
sandstone
limestone
pebble/cobble
basalt
KEY
Sandstone
Sandstone
Siltstone
Shale
Shale
Breccia
Conglome-rate
Basalt
Eroded
Limestone
Parallel lamination
Ripple
Trough cross bedding
Burrow/Roots
Soft sediment deformation
Flame/ball and pillow structure
Carbonaceous material
Mud rip up clast
Iron oxide concression
Stromatolite/microbial mat structure
Fish fossil
Caddisfly case
Oncoids

OUTCROP GEOLOGY

Mesozoic sedimentary basin fill deposits outcrop in a large area in the Tsagaansuvarga Basin (Fig. 2, 4). These Late Jurassic—Early Cretaceous strata lie unconformably on Paleozoic prerift successions, specifically upper Ordovician to Devonian intermediate grade metamorphosed (amphibolite phase), terrigenous sedimentary and volcanic units as well as their tuffs (Zabotkin et al., 1988, Ariunchimeg, 2011). The stratigraphic relationship between the Mesozoic and Paleozoic is mainly mapped as an angular unconformity; however, the contact is not well exposed in the area (Fig. 2, 3).

The main lacustrine to marginal lacustrine facies of the late Mesozoic basin fill were originally mapped and separately designated as the early Cretaceous Shinekhudag Formation, which is dominated by fine-grained mudstone lithofacies, and the overlying Huhteeg Formation, dominated by coarser-grained sandstone and conglomerate lithofacies (Fig. 3, 4; Zabotkin et al., 1988). However, the stratigraphic relationships and age constraints between these two formations are not well understood and they may reflect a time-equivalent facies variation of similar depositional systems (Johnson et al., 2014).

Prior to this study, the stratigraphic contact between the lower Cretaceous Shinekhudag and Huhteeg Formations was placed at the facies change between more

mudstone to sandstone dominated units, ~3093 m on our measured section (Fig. 4A; Zabotkin, 1988; 2013; Horton et al., 2013). This stratigraphic contact between the Shinekhudag and Huhteeg Formations has been reinterpreted to the 3448.5 m level, where a clearer depositional hiatus occurs, based on local geological mapping and depositional environment interpretations. A significant facies shift has been identified at this level from gray to tan colored, fine- to coarse-grained sandstone beds to the red-green mottled siltstone beds (Fig. 4A). The siltstone beds are generally massive, poorly cemented, and contain abundant coal fragments and coaly horizons. They are sporadically interbedded with thin (<5 cm) intensely eroded paleosol horizons. This red-green siltstone interval transitions into clast- to matrix-supported conglomerate dominated strata around 3450 m. The conglomerate beds are predominantly red to purple colored, clast- to matrix- supported, granular to pebble sized, poorly sorted, and range in size up to 10 m thick (Fig. 4A). Abundant trough cross beddings and clast imbrication can be found within these conglomerate beds.

Overall, these characteristics of the siltstone interval and overlying conglomerate dominated strata indicate alluvial depositional environments. We interpret the siltstone interval as a floodplain depositional environment, and the entire overlying conglomeratic succession as fluvial and alluvial fan deposits (Bridge, 1993; Miall, 1996). The facies juxtaposition between the floodplain siltstone and underlying sandstone beds at the 3448.5 m level suggests a period of aerial exposure, possibly an unconformity (Fig. 4A). Similar facies contrasts as well as indistinct, mappable seismic reflections were encountered in subsurface data collected from the adjacent Tugrug Basin (Fig. 1B), and are interpreted as a minor synrift nonconformity (Johnson et al., 2014).

Basalt samples from near the contact between Tsagaantsav and Shinekhudag Formations were dated at 144±6.0 Ma, and basalt flow samples within the lacustrine facies (~2075 m level) are 131.6±2.5 Ma, both using the Rb-Sr method on whole rock samples (Fig. 3; Tully et al., 2015). Additionally, well-preserved ostracods were recovered from one of the bioherm samples and most of them were estimated as Upper Tithonian to Lower Berriasian in age (Marius Stoica, written communication, 2016). Thus, the Shinekhudag Formation is Lower Cretaceous age based on the age controls presented above. Bioherms, which are the main focus of this study, are located within the Shinekhudag Formation. Thus the following facies descriptions highlight this part of the synrift succession (Fig. 4B,C).

FACIES ANALYSIS

The lower Cretaceous Shinekhudag Formation of the Tsagaansuvarga Basin includes a variety of mudstone and sandstone dominated facies that together record overall evolution of this lake basin. The main lacustrine-marginal lacustrine intervals occur between 1800-3440 m on the general compiled stratigraphic section and these represent two distinct facies associations as described below, in stratigraphic order.

Lower interval—Fluctuating profundal facies association

This interval (1800-2862 m) includes interbedded mudstone, siltstone, sandstone, limestone, conglomerate, and basalt flows (Fig. 4B). The fine-grained facies range from dark, mm to cm-scale, fine laminated mudstone and fissile shale to more massive dm-scale bedded mudstones and siltstones (Fig. 5A,B). The fine mm to cm-scale laminated mudstones and fissile shales are often organic rich, with sporadic plant fragments. Prior to this study, numerous mudstone samples were analyzed from this lower interval for source rock potential. Total organic carbon (TOC) results revealed that the mudstone facies are indeed rich in organic carbon, ranging from 1.60% to 10.26% TOC with an average value of 5% by weight (Tully et al., 2015).

The mudstone and siltstone units of the lower interval are commonly interbedded with fine- to coarse-grained, normally-graded, tabular sandstone as well as marl beds (Fig. 5C). The sandstone beds are up to 2 m thick, tan-brown colored, and contain

abundant ripple cross stratification as well as planar laminations. The marl beds are 0.2-2.0 m thick, tan-brown to pink colored, often have planar laminations, are laterally continuous, and are dolomitic in composition as they are weak to insoluble to dilute hydrochloric acid.

At the 2458 m level, there are multiple distinctive, resistant, tan-brown, convex upward, mound-shaped, patch reef-like carbonate bodies identified, which are bounded by discrete stratigraphic interval between thick organic-rich mudstones (Fig. 6). The contact between the mounds and the underlying oi-shales is abrupt with no indication of a subaerial exposure (Fig. 6A,B,C). The diameter of individual mounds is 0.5-2.0 m and their thickness ranges from 1-5 m. These mounds are concentrated within one stratigraphic interval, isolated from each other laterally by 30-40 m, and can be traced as an interval for more than 1 km along strike (Fig. 2). Internally, mounds are characterized by mm-scale wavy laminations and they contain ooids, oncoids, and abundant colonies of tube-shaped, cylindrical structures interpreted as insect cases due to their similarity to others that have been previously reported from the Eocene of North America and elsewhere (Fig. 6D,E,F; Leggitt et al., 2001; 2007). These insect cases can make up to 40% of the volume of a single mound (Fig. 6E).

The coarsest grained facies of the lower interval are characterized by granular to pebble sized, moderately to poorly sorted, matrix supported conglomerate beds, up to 3 m thick. The conglomerate beds characteristically lack sedimentary structures, except rare poorly defined planar cross beds. Between 2133 m to 2150.5 m, there is megabreccia with chaotic soft sediment deformation, which contains dismembered m-scale sandstone, mudstone, and dolomite boulders.

The volcanic components within this interval are mainly characterized by a single bed with flow texture and thin potential ash beds that are poorly preserved in outcrop (Fig. 5D). A 4 m-thick basalt bed with pillow texture is found near the base of the lower interval, located at approximately 2075 m on our measured section (Fig. 4B). The basalt bed has porphyry texture with plagioclase phenocrysts along with other fine mafic minerals.

Upper interval—Fluvial lacustrine facies association

This interval (2862-3440 m) is generally sandier in comparison to the lower interval. Overall, the interval consists of mudstone, siltstone, sandstone, and conglomerate (Fig. 4B). The fine-grained facies range from gray to dark gray colored, fine laminated mudstone to more massive siltstone beds. Horizontal burrowing and soft sediment deformation are pervasive throughout the mudstone and siltstone facies. The mudstone beds are siltier in composition and carbonaceous material rich compared to the lower interval. The fossil content of this interval is generally sparse except invertebrates such as ostracods and gastropods found within the mudstone and siltstone units, as well as unidentifiable, reworked plant fragments found within the sandstone units.

The mudstone and siltstone facies are commonly interbedded with tan-brown colored, fine- to coarse-grained sandstone beds. These units are typically normally-graded and moderately sorted with abundant trough cross bedding, climbing ripples, and soft sediment deformation as well as mud rip-up clasts. They commonly form lenticular bodies with erosive bases, up to 8 m thick and 12 m wide (Fig. 5E,F). The sandstone units typically overlie and locally scour into mudstone and siltstone units and a few

possible root casts are present at the 3381.5 m level. Overall, the thickness of the sandstone beds tends to increase from dm-scale to m-scale up section.

The coarsest grained facies of the upper interval consists of up to 10 m successions of gray colored, granular to pebble-cobble sized conglomerate beds containing quartzite, chert, argillite, sandstone, siltstone, basalt, and andesite clasts. These conglomerate beds are characteristically tabular to lenticular with sharp bases, and mainly overlie siltstone and mudstone beds. The tabular conglomerate beds tend to be matrix supported, massive, and poorly sorted, while the lenticular conglomerate beds are mainly clast supported and have trough cross beds as well as strong clast imbrications.

Sedimentary facies interpretation

The lower and upper intervals of the lower Cretaceous Shinekhudag Formation reflect two distinct lacustrine facies associations. Here we used the Carroll and Bohacs' (2000) three end-member lacustrine facies association classification and terminology to describe and interpret each.

The lower interval (1800 m-2862 m) (Fig. 4B,C) is assigned to the fluctuating-profundal facies association. The fine-grained facies of this interval includes finely laminated, organic rich mudstone, siltstone, and dolomitic marl beds with terrestrial and aquatic organic matter. These predominantly fine-grained, mudstone, and siltstone beds are consistent with the distal deep lake sediments resulted from the sediment suspension settling and traction deposition, thus we interpret them as a profundal offshore lake environment (Carroll & Bohacs, 1999; 2001; Tanavsuu-Milkeviciene et al., 2012). The fine, mm to cm-scale lamination and the high concentration of organic matter (average

5% TOC) preserved in this offshore mudstone facies is highly diagnostic of the anoxic hypolimnion part of a stratified lake environment (Carroll & Bohacs, 2000; Renaut & Gierlowski-Kordesch, 2010). The laterally homogenous, laminated marl beds interbedded with the mudstone and siltstone are interpreted as chemical sediments precipitated from Ca/Mg and HCO^3 bicarbonate rich lake water, within the clastic-input-starved offshore lake environment (Platt & Wright, 1991).

The mound-shaped carbonate units that are concentrated within a thick horizon of oil shale at 2458 m level (Fig. 4C) are quite enigmatic in terms of their depositional processes and relationships with the bounding facies. Their physical appearance, internal sedimentary structure, and relationship with the surrounding lithofacies suggested that these are bioherms, defined by Klement and others (1967) as “a massive mound shaped structure, that is discordant in relationship with the surrounding facies with different lithologic types”. Co-occurrence of the ooids and oncoids in these bioherms indicate a shallow water setting with wave modification, while the diagnostic traces of insects, the caddisfly cases, described further in the next section, indicate a well-oxygenated, nutrient rich environment, perhaps the littoral zone of the lake (Bohacs et al., 2007; Renaut & Gierlowski-Kordesch, 2010). Similar enigmatic relationships containing types of insect cases are found in other bioherms in modern and ancient examples (e.g., modern Great Salt Lake, Eocene Green River Formation; Loewen et al., 1999; Leggitt et al., 2001; 2007; Baskin, 2014).

The tabular sandstone facies in this interval (1800 m-2862 m) are consistent with distal turbidite beds, resembling a partial Bouma sequence that possibly resulted from a hyperpycnal plume, perhaps in a subaqueous prodelta environment (Fig. 5C;

Bhattacharya, 2006; Renaut & Gierlowski-Kordesch, 2010). The clast- to matrix-supported, poorly sorted conglomerate beds are interpreted here as mass transport deposits including high-density turbidites and debris flows, possibly in a subaqueous fan delta environment (McPherson et al., 1987; Nemec & Steel., 1988). The massive, matrix-supported, ~18 m thick megabreccia bed is interpreted as a large-scale debris flow deposit within a subaqueous landslide, perhaps resulting from a seismic event. The basaltic pillow lava flow (Fig. 5D) and cm-scale potential ash beds at the base of the section are possibly the result of a subaqueous volcanic extrusion: an indication of syndepositional magmatism.

Thus, we interpret the lower interval of the Shinekhudag Formation as mainly offshore lake sediments characterized by the fluctuating-profundal facies association (balance-filled lake basin type; Carroll & Bohacs, 1999; 2001; Renaut & Gierlowski-Kordesch, 2010). Possible distal fan delta beds encased in distal lake facies can be attributed to steep relief of the lake margin, which is a common feature in rift associated deep lakes (Cohen, 1989). The high topography of the lake margin possibly accelerated progradation of these fan delta beds, and they grade rapidly into offshore turbidites (Postma, 1990). Regional seismic sections from previous studies showed significant basin fill thickening away from the basin margin (Horton et al., 2013; Johnson et al., 2014), supporting the interpretation of a deep, stratified lake.

The upper interval (2862 m-3440 m) (Fig. 4B) of the Lower Cretaceous Shinekhudag Formation is assigned to the fluvial-lacustrine facies association, a combination of both offshore lake deposits, marginal proximal deltaic, and fluvial sediments. The lower portion of this interval (~2862 to 3148 m) is transitional with the

underlying fluctuating profundal facies association; it is characterized by fine-grained mudstone to siltstone dominated facies and gradually coarsens upward to sandstone dominated facies (~3148 to 3430 m; Fig. 4B).

The fine-grained facies of this upper interval are dominantly interbedded mudstone and siltstone beds characterized by tabular, laterally continuous beds with fine laminations as well as soft sediment deformation and ripple cross stratification. Compared to the underlying section, the upper interval contains more clastic-rich, silty mudstone with fewer laminated oil shale, and dolomite beds (Fig. 5E). In general, deposition of these units is dominated by both suspension settling and bedload transport, in a low-energy distal lacustrine environment. However, the internal sedimentary structures coupled with the vertical to sub-vertical burrowing of the siltstone units suggest a slightly higher energy environment than comparable facies in the lower interval. Thus, we interpret the fine-grained facies as a distal offshore lake deposit that was at least temporarily stratified but also periodically dominated by a higher energy subaqueous prodeltaic or fan delta environment (Nemec & Steel, 1988).

The sandstone beds of the upper interval represent fluvial channel fill, as indicated by their lenticular shapes, erosive bases, normal grading, common mudstone rip-up clasts, and both trough and planar cross bedding (Fig. 5E,F). The internal sedimentary structures and possible root casts are an indication of a high-energy fluvial-deltaic complex, or a delta front or shoreface depositional environment (Coleman & Prior, 1982; Miall, 1996). In comparison to the channelized sandstone units, the tabular, massive conglomerate beds within the mudstone and siltstone facies (e.g., 2970 m to 3070 m) are more consistent with the high-density turbidites and debris flow deposits,

possibly in a fan delta environment (Fig. 4B; McPherson et al., 1987; Bridge, 1993; Bhattacharya, 2006). Similar to the lower interval, these fan delta beds are possibly the subaqueous portion of an alluvial fan environment along a steep margin of the lake (Cohen, 1989; Postma, 1990).

The large-scale gradual transition of the basin fill lacustrine facies association from fluctuating-profundal (lower interval) to fluvial-lacustrine (upper interval) reveals progressive evolution of the lake basin as well as gradual shifting of the lake shoreline. The transition of the facies association is controlled by relative balance of sediment and water input versus potential accommodation (Fig. 4B; Carroll & Bohacs, 1999; 2000).

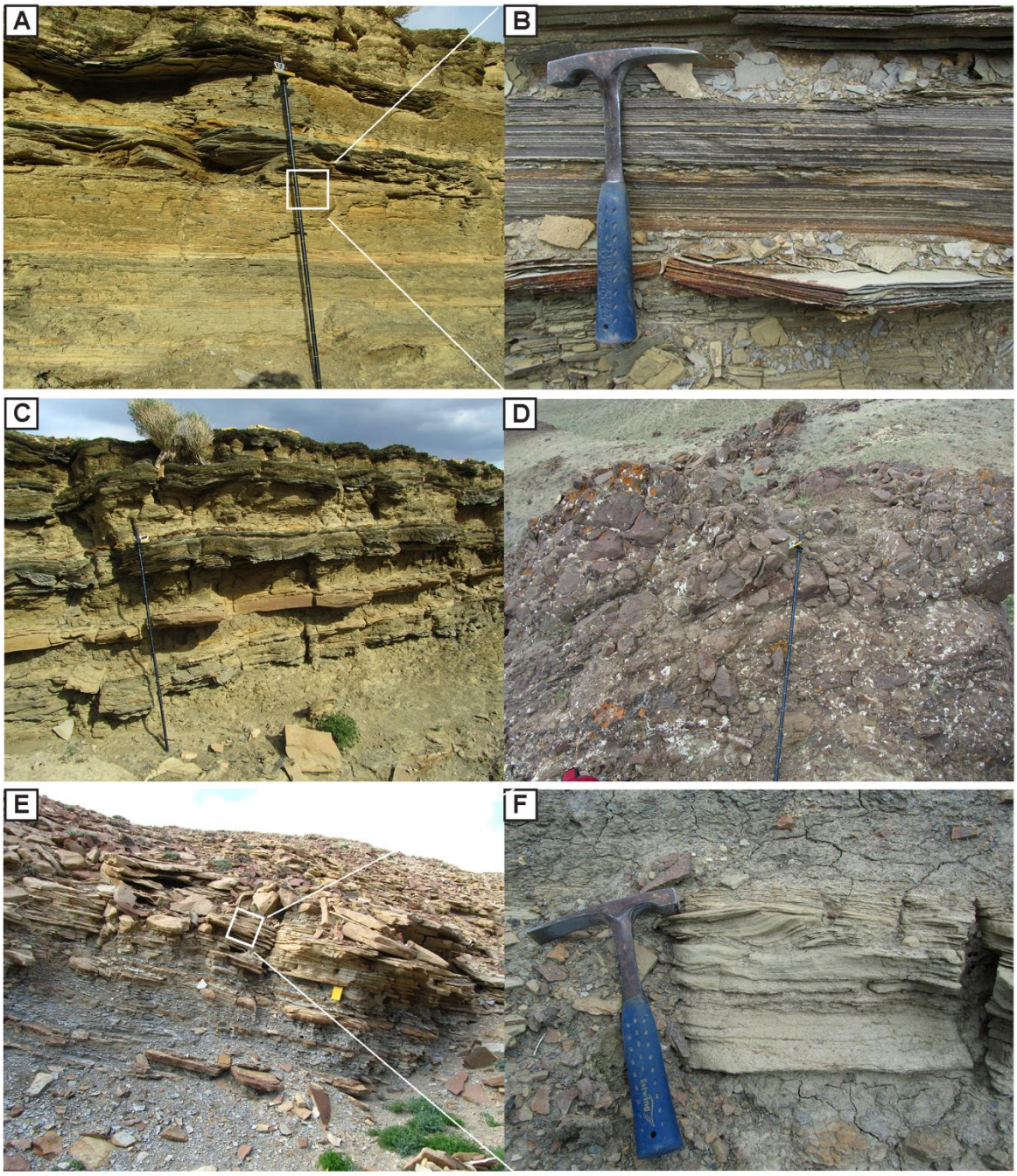

Figure 5. Photos of the main facies. (A) Laminated mudstone facies of the lower interval. (B) Close view of organic-rich, laminated mudstone. (C) Interbedded mudstone, tabular sandstone, siltstone, and marl facies. (D) Pillow lava of the lower interval. (E) Coarsening upward interbedded sandstone, siltstone, and mudstone facies within the upper interval. (F) Climbing ripples of the sandstone facies within the upper interval.

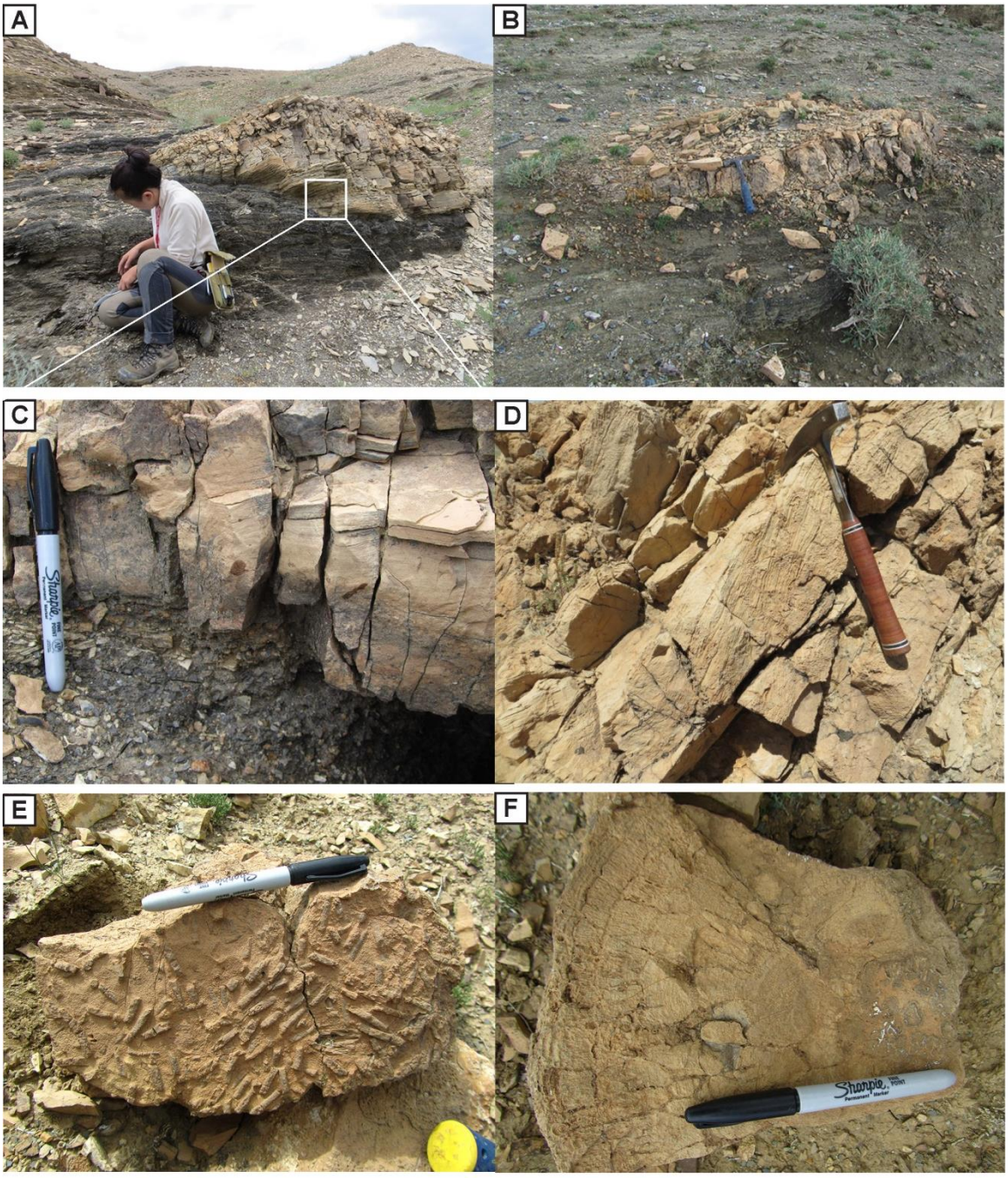

Figure 6. Field photos of the bioherms. (A) Mound-shaped bioherm bounded by laminated, organic-rich mudstone. (B) Mound-shaped bioherm bounded by laminated mudstone. (C) Contact between bioherm and underlying mudstone. (D) Wavy laminated structure of the bioherm. (E) Tube-shaped caddisfly cases on the weathered surface of bioherm. (F) Fine laminated internal structure of the bioherm.

BIOHERM ANALYSIS

The detailed morphologies of the Lower Cretaceous Shinekhudag Formation bioherms (measured at ~2458 m level; Fig. 2, 4C, 6) are described at three levels following the recommendations of Shapiro (2000). Macrostructures include bioherm geometry, dimensions, and outcrop expressions, as described under facies descriptions above. Mesostructural-level description includes the detailed studies of the internal bioherm fabrics in hand samples, and petrographic observations are the microstructural level of investigation.

Mesostructure

The 22 hand samples were classified following Dunham (1962). The majority (14) of the hand samples are packstones containing caddisfly cases as well as ooids and oncoids: they are grain-supported with both micrite matrix and calcite cement. Seven samples are boundstones, composed of mm-scale laminated carbonates, caddisfly cases, and other grains. One remaining sample is purely an oolitic packstone with no caddisfly cases, nor any microlaminated carbonate.

Caddisfly cases form up to 75% of the packstone sample volume, ranging from loosely to densely packed, along with other grains including ooids, oncolites, plant fragments, and rare clastic grains (Fig. 7). The caddisfly cases can be recognized easily

on the eroded surface of the hand samples, displaying a variety of morphologies (Fig. 7). The case shape varies with position relative to the eroded surface: they are round or circular shaped when perpendicular, elliptical when positioned obliquely, and cylindrical tube-shaped when they are parallel.

The sizes and shapes of the caddisfly cases are nonuniform on the hand samples. We measure a total of 115 caddisfly case sizes from their caudal to cephalic ends on the hand samples. Based on these measurements, their lengths and internal diameters have a progressively increasing trend, ranging between 7-21 mm and 1.5-2.5 mm, respectively (Fig. 8). The majority of the caddisfly cases are straight with no curvature along their long axes in most examples (Fig. 7); however, some are occasionally slightly curved along their long axes forming a "J" shape (Fig. 7). Based on their shape differences, we defined two types of caddisfly case distributions (Fig. 7, 8, 9).

Straight caddisfly cases. The majority of the caddisfly cases documented from the hand samples have straight cylindrical tube shapes (Fig 7A,B,C,D). The lengths and internal tube diameters of this type of cases vary, with their length ranging between 7-21 mm, and diameter ranging between 1.5-2.5 mm (Fig. 8). They are slightly tapered to their posterior ends and they are mostly visibly open to their anterior ends. These cases are mainly filled with calcite cement and can rarely be empty (Fig. 7A,B,C,D). The cases are lined with about 1 mm thick, dark brown to black colored organic carbonaceous materials interpreted as plant fragments as well as other minor grains (Fig. 7A,B,C,D). They occur with no to very minor degree of alignment and can be found with or without the other types of cases (Fig. 7A,B,C,D).

Curved caddisfly cases. The curved caddisfly cases are rare in comparison to the

straight cases. These cases are slightly curved along the long axis forming curved J-shapes (Fig. 7B,C,D,E,F). The lengths of the curved caddisfly cases range between 8-12 mm and diameters range between 1.5-2.1 mm (Fig. 8). They are slightly tapered to their posterior ends, but the anterior ends were not described due to their rareness. Abundance of this type of cases may be underestimated due to their similar appearance to the straight caddisfly cases in cross section and oblique view (Fig. 7B,C,D,E,F).These cases are commonly filled with carbonate mud and armored with thin calcite as well as dark colored plant fragments (Fig. 7B,C,D,E,F). The construction behavior of these cases is clarified by thin section description, below.

Microstructure

Sixteen standard and large format thin sections were analyzed for microstructure description; three of them were stained on ½ of the section with alizarine red S-dye for improved identification of carbonate mineralogy. All samples display original depositional fabrics with little impact of diagenesis except cementation, as described below. The majority (10) of the thin sections were prepared from the packstones that are composed of caddisfly cases (~75%) and various allochems (~25%). These samples show microscopic details of the main skeletal and non-skeletal grains of the packstone along with the fine-grained matrix, and cement (Fig. 10, 11). The remaining six thin sections are from the boundstones that are composed of fine laminated carbonate (~60%), caddisfly cases (~10%), and various allochems (~30%). These samples show clearly defined mm-scale microlaminated fabrics as well as association of both microlaminates and other grains including the caddisfly cases (Fig. 12). We describe detailed depositional

and diagenetic microfacies of the packstones and boundstones separately due to their compositional differences.

Depositional microfacies of the packstones. Here, we mainly focus on petrographic characteristics of the packstone grains and matrices. The grains of the packstones are predominantly composed of caddisfly cases and lesser amount of ooids, oncoids, plant fragments, ostracod valves, carbonate grains, as well as sporadic feldspar and biotite grains (Fig. 10, 11). The caddisfly cases and other allochems are packed together by massive microcrystalline micritic matrix (Fig. 10E,F). These matrices are mainly dolomitic in composition, as they show no staining from the alizarine red-S dye (Friedman, 1959; Dickson, 1966).

In thin section, caddisfly cases show tight to loosely packed, aligned to non-aligned caddisfly cases with some degree to no orientation pattern. Similar to the hand samples, caddisfly cases also display a variety of shapes in thin section: circles when they are cut perpendicular, ellipses when they are cut oblique, and long elongated ovals when they are cut parallel to their long axes (Fig. 11). These cases show a variety of materials incorporated for their case construction as discussed below.

Caddisfly case architecture. Around 90% of the caddisfly cases are strongly armored with diverse types of debris which cover most of their exteriors (Fig. 11A,B,C,D,E,G,H). The remaining 10% of the caddisfly cases are weakly armored with a few to no armor debris attached to the case exteriors (Fig. 11F). The caddisfly cases are mostly covered with an abundant amount of dark brown to black colored, almost opaque, thin, and elongated grains of plant fragments, a lesser amount of ostracod valves, subrounded carbonate grains, and occasionally fine- to very fine-grained detrital clastic

grains such as biotite and feldspar (Fig. 11). Plant fragments are the most abundant type of armor material, and about 30% of the plant fragments were originally wood pieces with diagnostic cellular structures (Fig. 11B,D). The remaining 70% of the plant fragment armoring has no identifiable structure (Fig. 11A,G,H). The average length of armoring plant fragments (n = 108) is 0.66 mm and the average thickness is 0.1 mm. Rarely, the woody armor materials reach up to 1.97 mm in length and 0.53 mm in thickness. The next most-common type of the caddisfly case armors are the ostracod single and intact valves (n=30), with average lengths of 0.58 mm and average thicknesses of 0.06 mm (Fig. 11B,C). Additionally, elongated, dark brown colored, pleochroich biotite grains (n=12) form a minor component of case armor material, with average lengths of 0.26 mm, average widths of 0.04 mm, and rare feldspar grains (n=8) with average lengths of 0.37 mm and average thicknesses of 0.20 mm (Fig. 11E,G).

Diagenetic microfacies of the packstones. The main diagenetic microfacies criteria are cements, neomorphic alterations, dissolution features, and fracturing (Scholle & Ulmer-Scholle 2003; Flügel, 2010). However, no alteration, dissolution, and fracturing features associated with the packstones were documented, thus cementation is the main point of description. The main types of porosities of packstones include the interparticle porosities observed between caddisfly cases and other allochems as well as the intraparticle porosities observed within the interiors of caddisfly cases (Fig. 10, 11; Choquette et al., 1970). Both of these types of porosities are filled with various-sized sparry calcite cements. The original interparticle pore spaces are chiefly cemented by the fine- to medium-grained calcite spars (Fig. 10A,B, 11F,G). The intraparticle pore space of the interior of the caddisfly cases are filled with coarse-grained blocky calcite cements

with distinct crystal boundaries (Fig. 11F). All these cements are presumably dolomitic in composition, as they show no staining from the alizarine red-S dye (Friedman, 1959; Dickson, 1966). However, no prevalent dolomitic textures were observed within these cements in the thin sections.

Depositional microfacies of the boundstones. The main focus of the boundstone microfacies description was the mm-scale microlaminated micrite component. In thin section, the microlaminated micrite fabrics are mainly defined by irregular alterations of wavy, crinkled to semi-crinkled laminations of dark green-brown colored micrite to light brown colored sparry calcite layers (Fig. 12). These laminations formed relatively flat to finger-like, microdigitate columns (4-12 mm in width and 6-17 mm in height) and cones with high angle inclinations as well as sphere-shaped oncoid fabrics in thin sections (Fig. 12B,C,G,I). The average diameter of oncoids is about 4 mm and composed of layers of wavy, semi-crinkly microlaminations (Fig. 12G,I). The microlaminations tend to drape and pinch out towards the steeply inclined sides of the columns and cones (Fig. 12B,C,D,E,F). These microlaminates are commonly associated with other grains during their sedimentation, such as binding and trapping particles between layers, growing around caddisfly cases, and reworking detrital grains into nucleation sites for oncoids (Fig. 12B,H,F,I). Occasionally, dark brown to almost black colored, very fine-grained, sphere shaped particles are bound between the layers of microlaminations, especially on the high angle, inclined surfaces. These particles may result from carbonate mud flocculations (Fig. 12F; Schieber et al., 2013). Also, oval to circular-shaped caddisfly cases are documented within the interior of these microlaminates (Fig. 12B,H). Additionally as with the armored casings, various types of grains (e.g., ostracod, plant

fragments, and detrital feldspar grains) are accumulated between the dome, cone, and sphere-shaped microlaminated micrite growths (Fig. 12B).

Diagenetic microfacies of the boundstones. Similar to the packstones, no alteration and fracturing features associated with the microlaminates were observed in thin sections. Therefore, cementing and dissolution history was our main descriptive focus. The main types of porosities of the boundstones include primary shelter porosities associated with the microlaminates, and secondary vugular porosities associated with the dissolution fabrics (Fig. 12B,C,J,K,L,M; Choquette et al., 1970).

Primary shelter porosities between the microlaminates are mostly half dome shaped and filled with 2-3 stages of cements in the following order: (1) isopachous calcite cement & fibrous calcite; (2) gypsum or (1) isopachous & fibrous calcite; (2) gypsum; (3) granular microspar (Fig. 12C,J,K). The first stage of the cement between shelter porosities includes needle-like, fine to medium-crystalline fibrous calcite as well as subhedral, medium-crystalline isopachous calcite cements. They fully line the interior of the pore spaces with 0.05 to 0.1 mm thicknesses (Fig. 12J,K). The second stage of the cement between the shelter porosities is characterized by euhedral to subhedral, low-relief, and platy crystals of gypsum, with diameters ranging 0.06 to 0.25 mm (Fig. 12J,K). Granular calcite microspars, the last stage of the cement, are crystallized between the preceding calcite and gypsum cements (Fig. 12K).

Secondary porosities found within the thin sections are often associated with the microlaminated fabrics as a result of dissolution. They are predominantly characterized by various sized, irregular vug shapes, with diameters ranging from 0.09 to 2.0 mm. (Fig. 12B,L,M). These secondary pore spaces are mainly partially rimmed with a single stage

of the isopachous calcite cements. Occasionally, they are fully filled with isopachous, as well as blocky calcite cements (Fig. 12L,M).

As indicated by the staining method, the primary pore space filling cements are presumably dolomitic in composition in comparison to the secondary pore space filling cements (Fig. 12M; Friedman, 1959; Dickson, 1966). However, we did not observe clear dolomite textural fabrics within these cements similar to the packstone samples.

Mesostructure and microstructure interpretation

The co-occurrence of the traces of aquatic insects (caddisfly) and microorganisms on the hand samples and thin sections reveals that the Shinekhudag Formation bioherms are predominantly controlled by the interaction of two distinct biologic communities. We interpret the main depositional controls of these bioherm forming components (caddisfly cases and microbialites) based on the depositional microfacies description of the packstone and boundstone samples.

The development of each caddisfly case is primarily controlled by the behavior of an individual larva/pupa (Wiggins, 2004). The cases were built by the larvae/pupae to protect themselves from predators and to enhance their respiration efficiency, similar to their modern analogues (Wiggins, 2015). The geometry and architectural analysis of hundreds of caddisfly cases reveals that the Cretaceous Mongolian caddisflies constructed cylindrical tube-shaped cases during their larval stage using bits of debris from the surrounding environment (Holzenthal et al., 2007; Statzner et al., 2011). Although the construction materials of the caddisfly cases are dominated by plant fragments (e.g., woody barks, branches, and leaves), they also incorporated other

carbonate as well as clastic grains (e.g., ostracod valves, carbonate rock fragments, biotite, and feldspar), resulting in the complex architecture of cases (Fig. 9). Therefore, evidently the particles incorporated in the caddisfly case construction are a function of availability of materials in the surrounding lacustrine environment, thus they are the direct indication of paleoenvironment composition.

The two types of caddisfly case morphologies identified in hand samples and thin sections likely belonged to the same family of caddisfly since they all have prominent tubular shape and similar case architecture (Wiggins, 2004; Fig. 7, 9, 11). However, the progressively increasing size trends of these caddisfly cases (Fig. 8) possibly reflect the size of the larvae/pupae that built and owned them (Holzenthal et al., 2007). Thus, we argue these continuum increased sizes of the caddisfly cases represent growth stages of the caddisfly larvae (Wiggins, 1998). Most modern caddisflies undergo four distinct case-building larval stages, prior to their pupal stage and emerging as an adult insect (Wiggins, 2015).

The microfacies of the microlaminated micrite component reveal their primary depositional processes and controls. The laminated fabrics of the carbonates are always ambiguous in terms of the dominating controls on their sedimentation (Semikhatov et al., 1979; Burne et al., 1987; Riding, 2000; Frantz et al., 2015). However, there are accretions of wavy, crinkled to semi-crinkled laminations, which form various shaped fabrics including spherical oncoids, finger-like columns, and cones with high inclination angles (Fig. 12). Additionally, they trapped and bound flocculated micrite grains on their inclined surfaces, suggesting an adhesive chemistry (Meadows et al., 1994; Frantz et al., 2015). A combination of these characteristics is highly indicative of a biotic fabric and

thus, we conclude these microlaminates of the Shinekhudag Formation are primarily controlled by biologic activities rather than physical controls (Riding, 1991; 2000; Flügel, 2010). We interpret these microlaminated fabrics as the microbialite or stromatolites, which were predominantly accreted by the interaction of microorganisms, perhaps filamentous cyanobacteria and/or algal mats (Burne et al., 1987; Riding, 1991; Flügel, 2004; Frantz et al., 2013; 2015).

The diagenetic microfacies of the packstones and boundstones reveal the alteration processes associated with lithification of the bioherm (Flügel, 1982). The main diagenetic features of the packstones include primary interparticle and intraparticle pore spaces and their associated cements (Fig. 10A,B,E, 11F). By contrast, the main diagenetic features of the boundstones include primary shelter and secondary vugular porosities and their associated cements (Fig. 12B,C,J,K,L,M).

We interpret both the inter- and intraparticle porosities of the packstones, as well as shelter porosities of the boundstones, as syndepositional, developed during the deposition of the bioherms (Choquette et al., 1970; Chafetz, 2013; Mancini et al., 2013). The interparticle porosities are developed within the original pore spaces between caddisfly cases and other allochems of the packstones (Fig. 11B,F). The intraparticle pore spaces are developed within the interiors of the empty caddisfly cases (Fig. 11F). Alternatively, the shelter porosities observed within microbialites are potentially resulted from the decay of bacteria (Fig. 12B,C,J,K).

These primary pore spaces are filled with various types and stages of cements. Both the inter- and intraparticle porosities are completely filled with a single stage of fine- to coarse-grained, blocky calcite spars (Fig. 10A,E,11F). Additionally, the primary

shelter porosities are filled with generations of cements including isopachous and fibrous calcite rims, evaporate gypsum, as well as granular microspar cements (Fig. 12J,K). We interpret these cements to be precipitated immediately after deposition of the preceding growth of the microbialites. Evidently, all these primary pore space filling cements are syndepositional to early diagenetic as they are filling the primary pore spaces. Thus, we argue that these cements are potentially precipitated from subsequent carbonate-rich lake waters above the sediments that buried the bioherms (Thompson & Ferris, 1990; Dupraz et al., 2004). The precipitation of different types of cements with respect to their chemical compositions (carbonate versus evaporitic gypsum cement) is possibly a result of the changes in the environment, particularly lake water chemistry (Kelts et al., 1978; Eugster et al., 1983; Schnurrenberger et al., 2003).

Arguably, the secondary vugular porosities within the thin sections are developed during late diagenesis, a result from the changes in the environment enhancing dissolution processes (Fig, 12B,L,M; Choquette et al., 1970; Ali et al., 2010). The associated isopachous calcite and blocky calcite cements are potentially a result of meteoric diagenesis (Scholle & Ulmer Scholle, 2003; Flügel, 2010).

The mineral composition of the pore space filling cements (i.e., syndepositional, early diagenetic, and late diagenetic) is identified through the thin section staining method, and it indicates that the syndepositional to early diagenetic cements as well as the matrices of the bioherms are mainly composed of dolomites in contrast to the late diagenetic cements that are composed of calcites (Fig. 12M). This compositional variation demonstrates that the dolomitization processes have altered the bioherms prior to the late diagenesis. Considering the absence of dolomite textures within the thin

sections, the dolomitization process have occurred chiefly through a mimetic replacement, preserving the original calcite textural fabrics (Sibley, 1987; 1991; Braithwaite, 1991).

Figure 7. Caddisfly cases on the hand sample photos. (A) Straight (black arrow) caddisfly cases on the hand sample. (B) Straight (black arrow) and curved (white arrow) caddisfly cases on the hand samples. (C) Straight (black arrow) and curved (white arrow) caddisfly cases on the polished sample. (D) Straight (black arrow) and curved (white arrow) caddisfly cases on the polished sample. (E) Curved (white arrow) caddisfly case on the polished sample. (F) Curved (white arrow) caddisfly case on the polished sample.

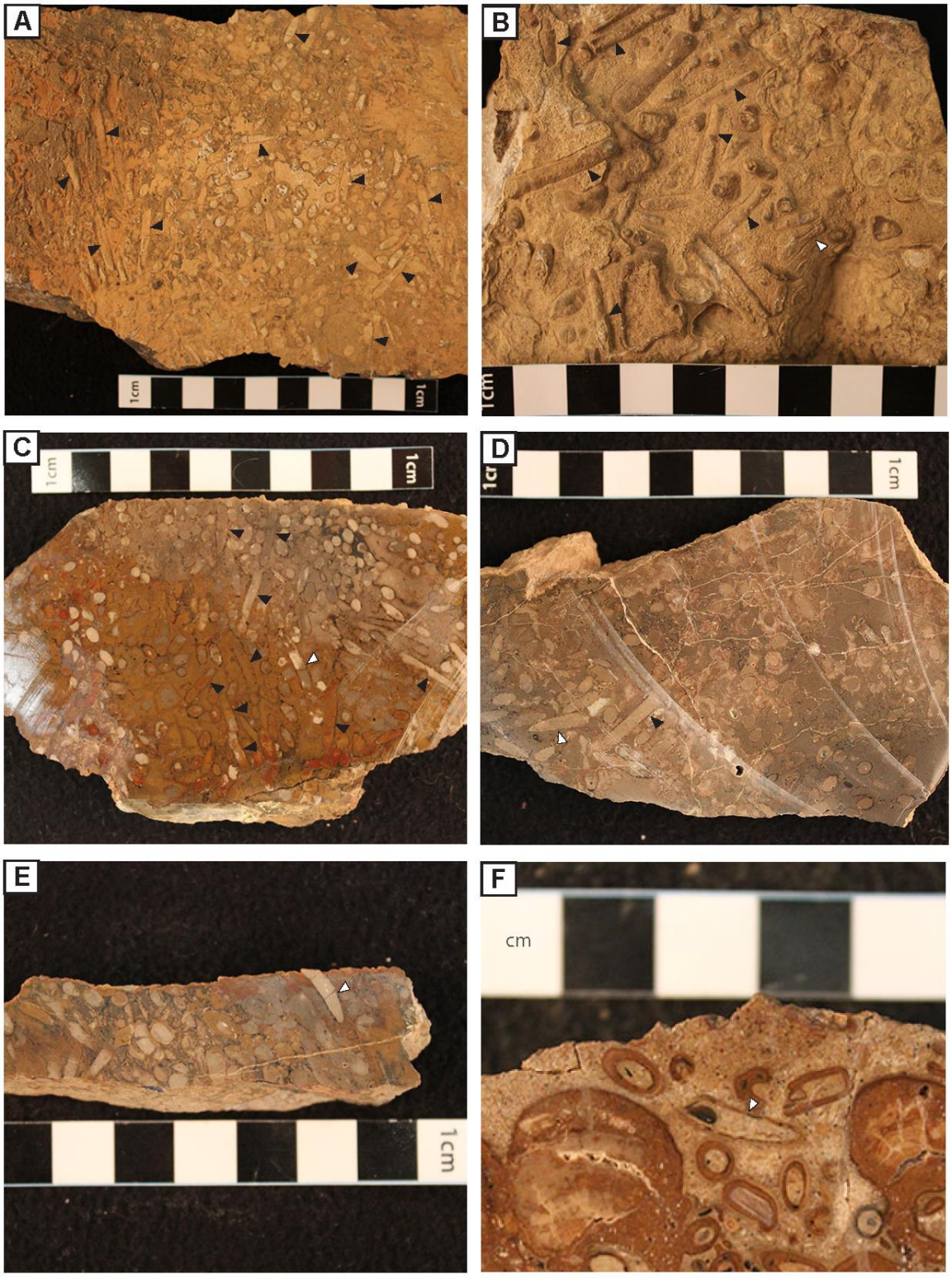
A
1cm
1cm
B
1cm
C
1cm
1cm
D
1cm
E
1cm
F
cm

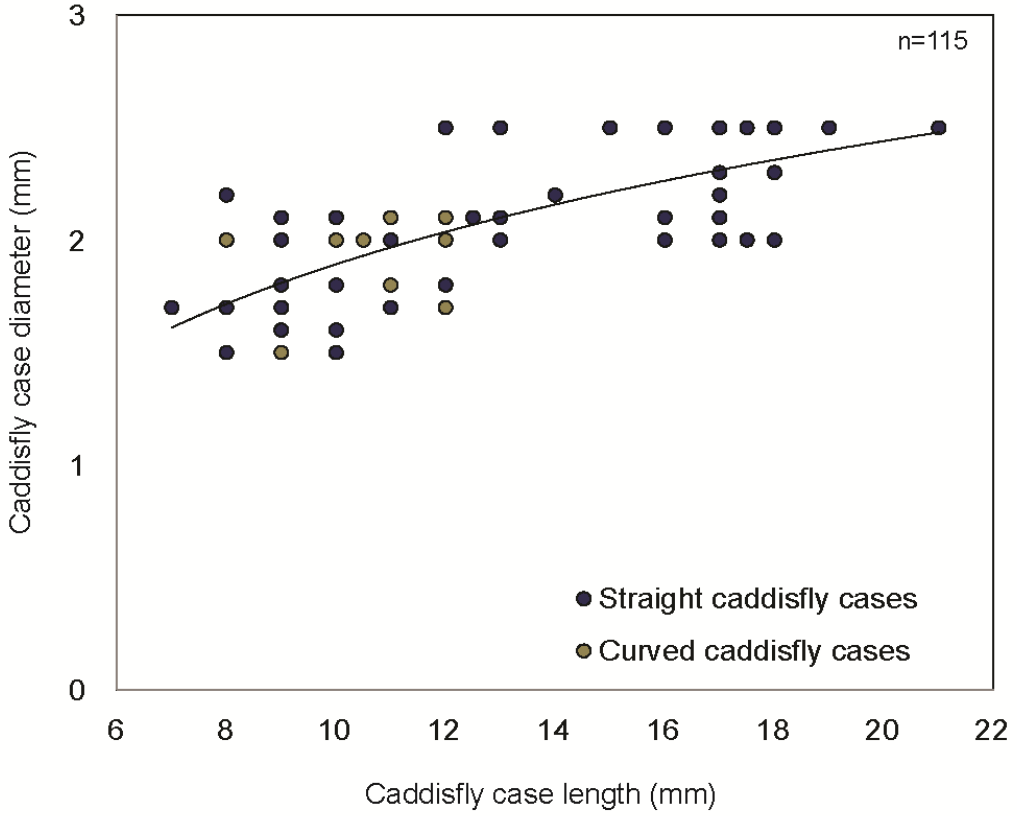

Caddisfly case characteristics	Length (mm)	Diameter (mm)	Percentage
Straight caddisfly cases	7-21	1.5-2.5	89
Curved caddisfly cases	8-12	1.5-2.1	11

Figure 8. Caddisfly case types and their size variations.

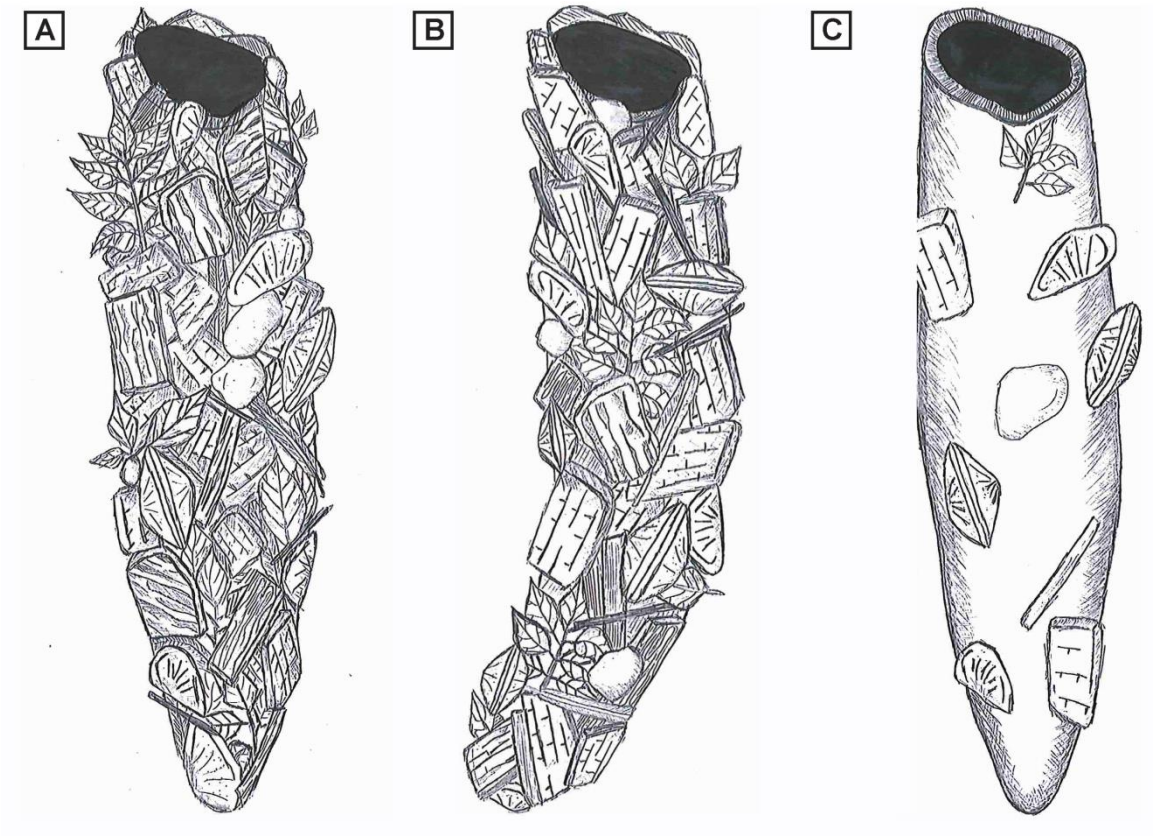

Figure 9. Caddisfly case reconstruction. (A) Straight caddisfly case. The case is strongly armored with plant fragments, ostracod valves, mica, and carbonate rock fragments. (B) Curved J-shaped caddisfly case. The case is strongly armored with plant fragments, ostracod valves, mica, and carbonate rock fragments. (C) Straight caddisfly case. The case is weakly armored with plant fragments, ostracod valves, mica, and carbonate rock fragments. Note: Caddisfly case armor are for illustration purpose, not in scale.

Figure 10. Photomicrographs of the packstone. (A) Allochems of the packstone cemented by fine-medium sparry calcite. (B) Intact ostracod allochem. (C) Detrital feldspar. (D) Gastropod. (E) Contast showing massive micrite matrix and various-sized calcite cement of packstone. (F) Massive micrite matrix. Abbreviasions: CC-caddisfly case; Fs-feldspar; Os-ostracod;Ga-gastropod;Ca-calcite;Mi-micrite; Pl-plant fragment.

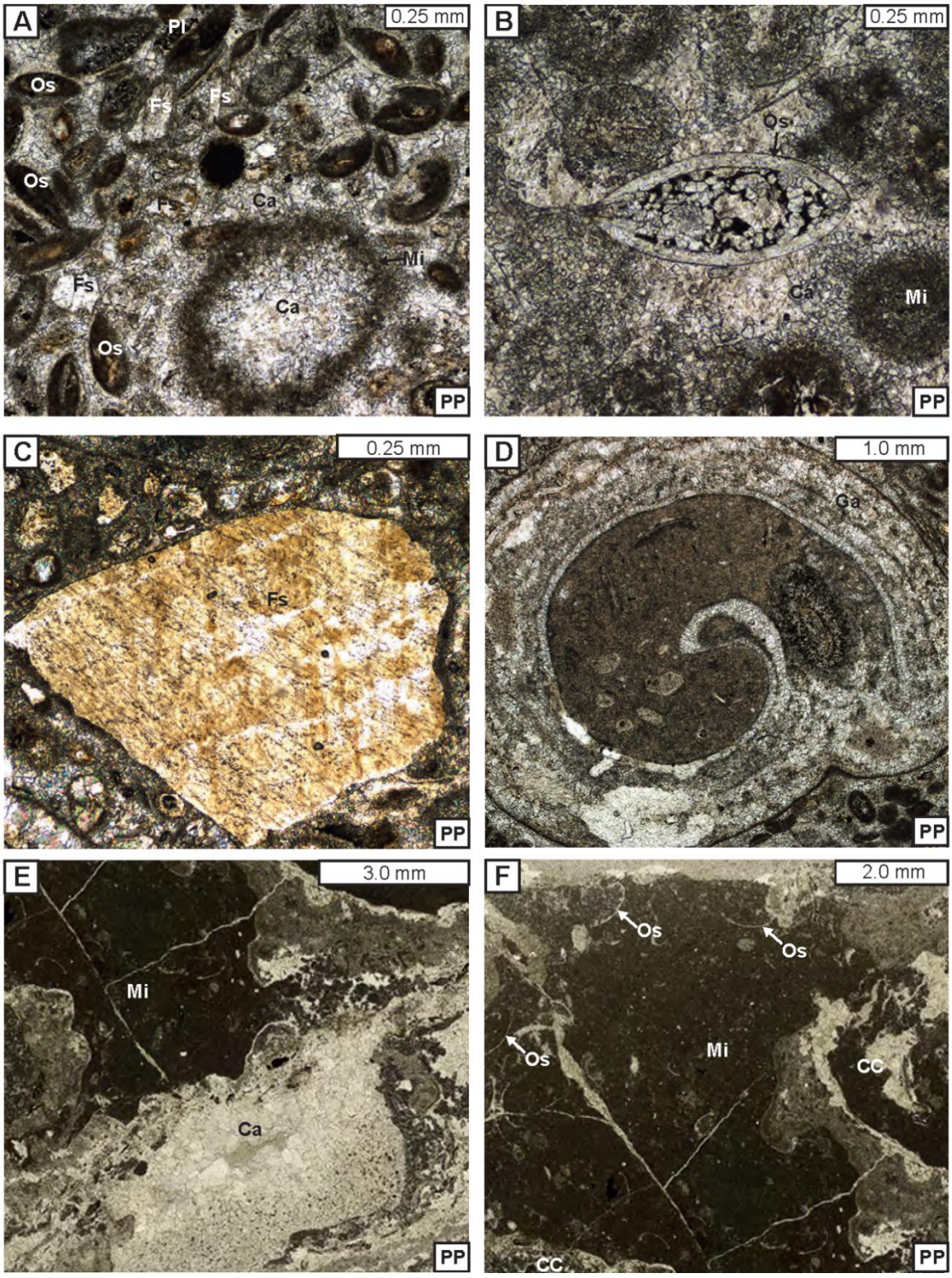
A
0.25 mm
Pl
Os
Fs
Fs
Os
Fs
Ca
Mi
Fs
Ca
Os
PP
B
0.25 mm
Os
Ca
Mi
PP
C
0.25 mm
Fs
PP
D
1.0 mm
Ga
PP
E
3.0 mm
Mi
Ca
PP
F
2.0 mm
Os
Os
Os
Mi
CC
CC
PP

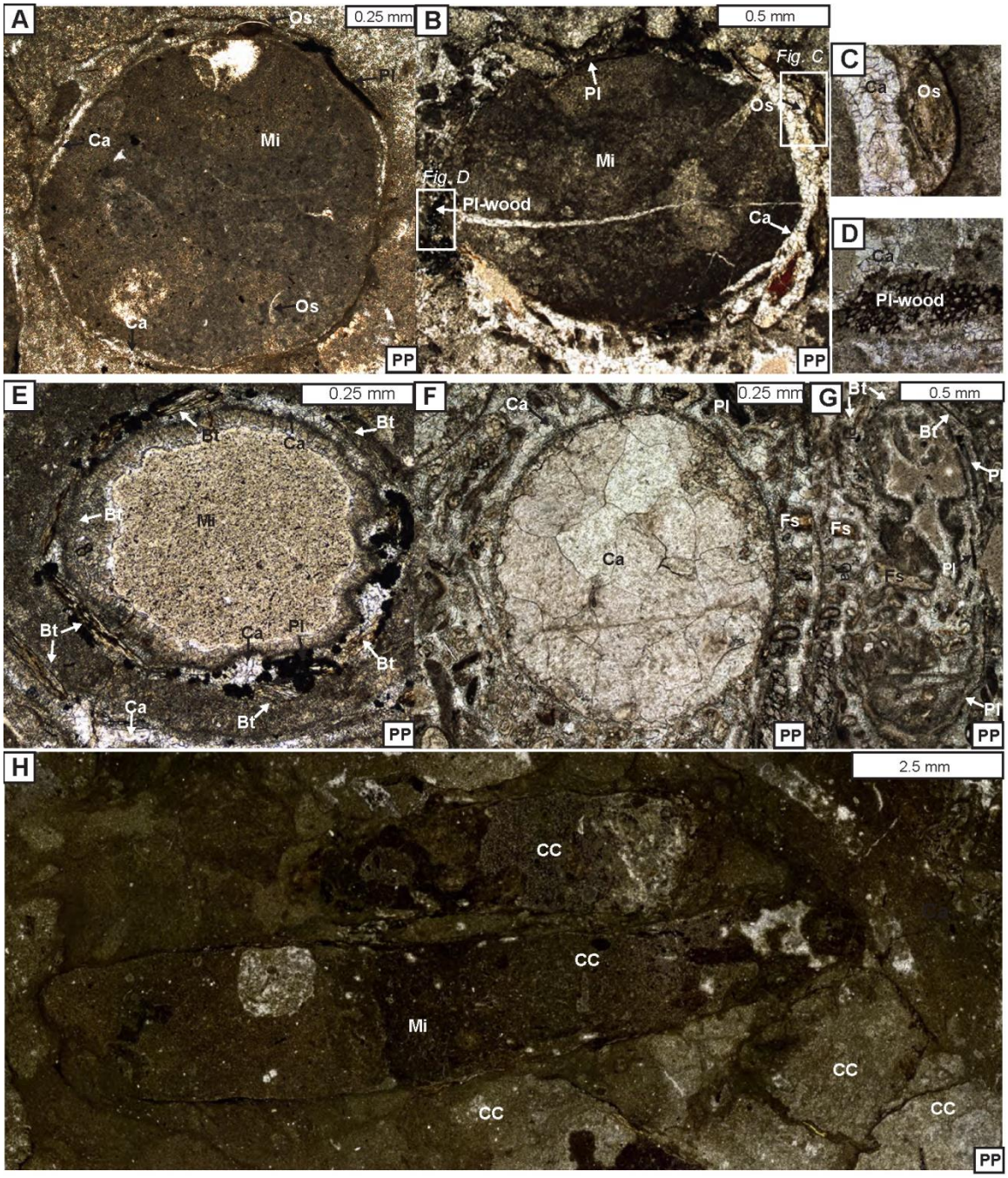

Figure 11. Photomicrographs of the caddisfly cases. (A) Caddisfly case in cross section. (B) Caddisfly case in cross section. (C) Close view of an ostracod armor. (D) Close view of a plant-wood fragment. (E) Caddisfly case in cross section with biotite armories. (F) Caddisfly case in cross section, filled with blocky calcite spar cement. (G) Oblique view of caddisfly case. (H) Caddisfly case in longitudinal section. Abbreviations: Ca-calcite; Mi-micrrite; Pl-plant fragment; Os-ostracod; Bt-biotite; Fe-feldspar; CC-caddisfly case.

Figure 12. Photomicrographs of the microlaminated micrites. (A) Hand sample photo of the boundstone. (B) Microlaminated micrite forming finger-like columnar fabrics. (C) Cone shaped microlamination. (D) Crinkled, wavy lamination with inclined surface. (E) Crinkled, wavy lamination. (F) Flocculated micrite grain trapped/bound between laminations. (G) Sphere shaped oncoidal fabric in cross section. (H) Caddisfly case bound by fine laminations. (I) Sphere oncoidal fabric with plant nuclei. (J) Shelter porosity and its associated cements. (K) Shelter porosity and its associated cements. (K) Shelter porosity and its associated cements. (L) Vugular porosity. (M) Vug porosity and its associated cements. Abbreviations: CC-caddisfly case; ML-microlaminated micrite; Mi-micrite matrix; SP- shelter porosity; VP- vugular porosity; OC-oncoid; FM- flocculated micrite; MS- granular microspar; IC-isopachous calcite; BC- blocky calcite; Gy- gypsum; Fi- fibrious calcite.

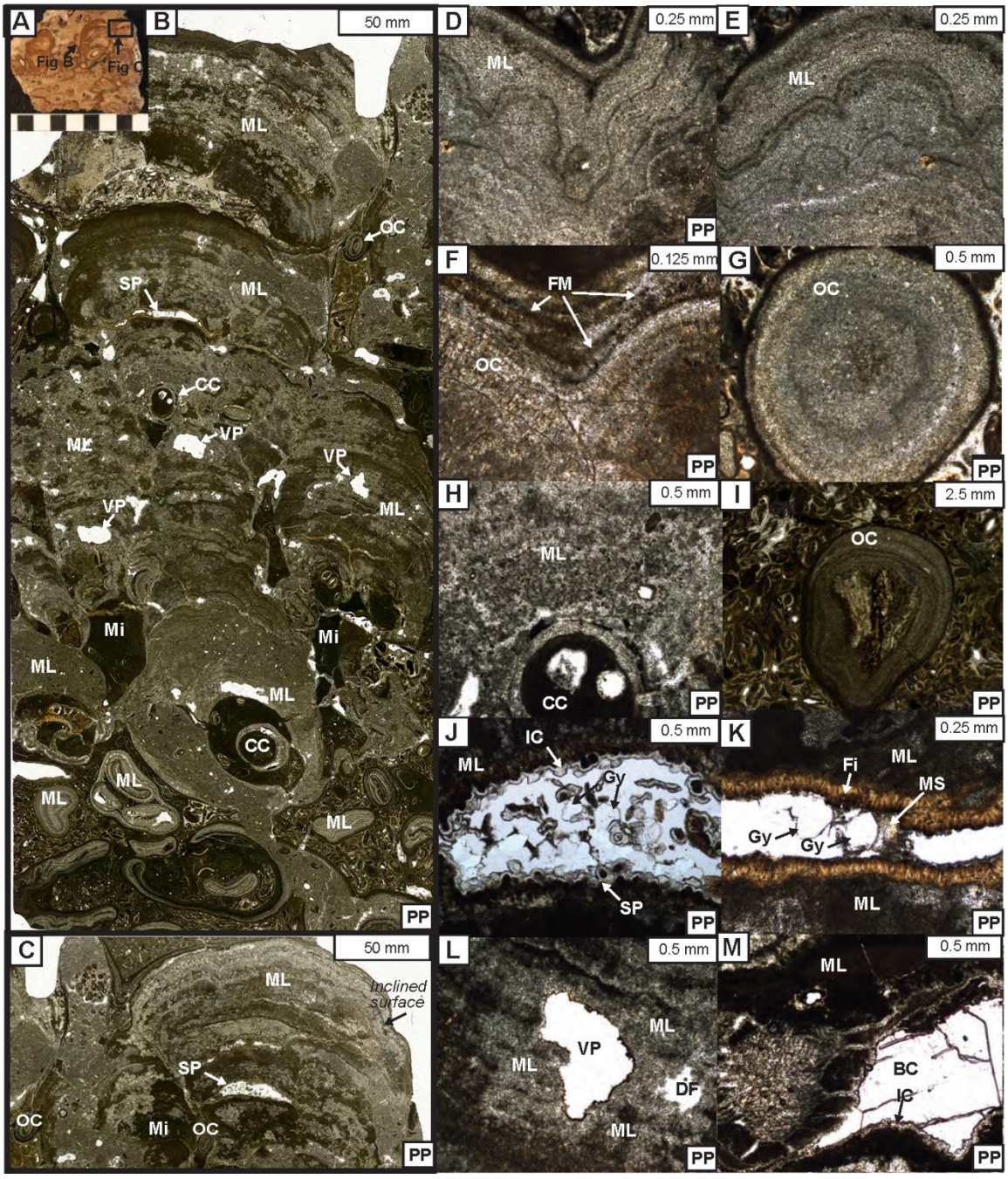
A
Fig B
Fig C
B
50 mm
ML
GC
SP
ML
CC
VP
ML
VP
VP
ML
Mi
Mi
ML
ML
CC
ML
ML
ML
PP
C
50 mm
ML
Inclined surface
SP
OC
Mi
OC
PP
D
0.25 mm
ML
PP
E
0.25 mm
ML
F
0.125 mm
FM
OC
PP
G
0.5 mm
OC
PP
H
0.5 mm
ML
CC
PP
I
2.5 mm
OC
PP
J
0.5 mm
IC
ML
Gy
SP
PP
K
0.25 mm
Fi
ML
MS
Gy
Gy
ML
PP
L
0.5 mm
ML
VP
ML
DF
ML
PP
M
0.5 mm
ML
BC
IC
PP

DISCUSSION

Evolution of the Tsagaansuvarga Basin (Late Jurassic through Early Cretaceous)

Widespread extension defined the main tectonic regime of eastern Mongolia and China during late Mesozoic time, expressed by nonmarine rift basins, bimodal volcanics, and associated metamorphic core complexes across the region (Traynor & Sladen, 1995; Webb et al., 1999; Graham et al., 2001). These extensional basins are well preserved in the subsurface and partially exposed where they have been inverted by younger faulting events (Johnson et al., 2004). Rifting in southeast Mongolia was active from at least 155–126 Ma based on $^{40}Ar/^{39}Ar$ dating of ash beds in synrift fill (Graham et al., 2001; Johnson et al., 2004).

Although late Mesozoic rifting is well known in eastern Mongolia and China, the western continuation of the extensional province is more enigmatic, particularly in northwest China where Jurassic-Cretaceous contraction is documented (Zheng et al., 1996; Dumitru & Hendrix, 2001; Vincent & Allen, 2001). Late Mesozoic extension is now documented in the Gobi-Altai of western Mongolia, including the study area in the Tsagaansuvarga Basin (Fig. 1: Cunningham, 2010; Johnson et al., 2014). Extension in this area is largely coeval with the East Gobi Basin based on closely related structural style, correlative ages of the basin fill (126-155 Ma), and similar stratigraphic relationships (Fig. 3; Graham et al., 2001; Johnson, 2004).

Large lake systems are recorded in thick (>2 km) synrift basin fill across the region; these deposits include oil shale intervals geochemically linked to produced oil, as well as synrift reservoirs largely in basin-margin clastic facies (Johnson et al., 2003; Prost, 2004; Tully et al., 2015). Broadly, synrift basin fill of the Tsagaansuvarga Basin gradually transitions from the lower interval, characterized by fluctuating-profundal facies association, to the upper interval, characterized by fluvial-lacustrine facies associations (Fig. 4, 5).

Internally, the lower interval contains distal mudstone and oil shale beds interbedded with thin carbonates, turbidite sandstones, poorly sorted fan delta deposits, as well as littoral-zone bioherms, together displaying a thick aggradational stacking pattern. Such heterogeneous lithology types, deposited in a distal to littoral lacustrine environment, suggest the lake was deep (Neal et al., 1997; Carroll & Bohacs, 2000; Renaut & Gierlowski-Kordesch, 2010). The proximal alluvial fan deltas, interbedded with distal lake deposits, indicate steeply dipping topography, potentially along a basin-bounding normal fault (Bull et al., 1972; Postma, 1990; Wells et al., 1999). A normal fault outcrops along the eastern margin of the basin and is juxtaposed with the offshore lake deposits, although its kinematics and relationship to the lake basin have not been fully investigated (Fig. 2). Based on these lines of evidence, we interpret the lower interval was deposited in balance-filled, deep lake basin.

The overlying upper interval is distinguished from the underlying interval by an increase in bioturbation, a decrease in calcareous material, and higher energy sedimentary structures (Fig. 4B, 5E,F). This interval is also chiefly characterized by mudstone, siltstone, sandstone, and conglomerate beds. However, facies associations of this interval

display a well-expressed progradational stacking pattern, indicating an increase in the sediment supply to accommodation ratio (Fig. 4B; Carroll & Bohacs, 1999; 2000). We therefore interpret the upper interval as deposited in an overfilled lake basin with open hydrology, which resulted in increased clastic grain size of the basin fill.

The change in depositional environments between the lower and upper intervals reveals the evolution of the lake basin type. Over time, the basin responded to the changing balance of main sedimentation controlling factors: potential accommodation space and sediment and water input (Carroll & Bohacs, 1999; 2000). The high potential accommodation and high sediment/water input during deposition of the lower interval resulted in a regional shoreline transgression and a balance-filled lake basin. This stage may coincide with a peak-rift time of ~133-126 Ma when subsidence rate was high and basin accommodation was increasing (Johnson, 2004). Concurrently, the humid, subtropical climate was supplying sufficient sediment and water into the catchment area to balance the increased accommodation space (Keller & Hendrix, 1997; Johnson et al., 2004). In contrast, the lower potential accommodation and unchanged high sediment/water input during the deposition of the upper interval resulted in basinward-progradation of the shoreline, or an overfilled lake basin. This stage may coincide with an early rift-sag phase, when subsidence of the catchment area was decreasing and eventually overtaken by the continued high sediment and water input.

Development model of the bioherms

We argue that the bioherms of the Lower Cretaceous Shinekhudag Formation developed as a result of symbiosis of two main biological communities: caddisfly

larvae/pupae and microbialites. Together they played principal roles in the deposition of these bioherms similar to well-studied lacustrine bioherm examples in the western US, particularly the Eocene Green River Formation (Loewen et al., 1999; Leggitt et al., 2001; 2002; 2007).Therefore, we suggest naming them “microbial-caddisfly bioherms”. Both biogenic factors are equally important for understanding the development of microbial-caddisfly bioherms and both are controlled by ecological and environmental factors.

Prior to this study, a development model of similar microbial-caddisfly bioherms was constructed, mainly focusing on the Eocene Green River Formation in North America (Buchheim et al., 2012; Awramik et al., 2015). The bioherms of the Green River Formation are composed of repeated rhythmic alternations of the well-arranged and uniformly-sized caddisfly cases and mm-scale microbial laminations (Loewen et al., 1999; Leggitt et al., 2002; 2007). Leggitt and others (2001) rooted this association fundamentally to the biological behaviors of the caddisfly larvae/pupae and microorganisms. Modern caddisfly pupae communities often become coordinated and arrange their cases only during the annual pupation event (Wiggins, 2004). Based on modern behavior, Leggitt and others argued that Eocene caddisflies similarly arranged their uniform-sized cases during yearly pupation events. After each pupation event, benthic microbialites grew on the empty case aggregates, slowly taking over the role of the bioherm development until the next caddisfly pupation event. A combination of these repeated actions have resulted in the complex microbial-caddisfly couplet bioherms found in the Green River Formation (Fig. 13A; Leggitt et al., 2001; 2007).

Despite their similarities, there are notable differences in the Mongolian examples. In the Cretaceous Shinekhudag Formation, caddisfly cases are sub-aligned to

unaligned, reflecting poorly organized or unorganized biotic action during bioherms development. The progressively increased size trends of these caddisfly cases reflect different growth (instar) stages of caddisfly larvae. Based on the biology of caddisfly larvae/pupae, the aggregations of nonuniform-sized empty cases reveal case-abandonment behavior during larval/instar stage (Lloyd, 1921). Non-cyclic alternations of Mongolian caddisfly cases and associated microbialites are notably different than the Green River Formation couplets, as seen in thin section (Fig. 12B). Instead, Shinekhudag Formation bioherms are typically preserved as aggregations of microbial laminae-bound caddisfly cases, without systematic cyclic alternations. Due to these contrasting characteristics, the development mechanisms of the Shinekhudag Formation bioherms require a different interpretation than in the Green River Formation.

Based on the paragenetic relationship of the main bioherm building components including the grains, matrices, and generations of cements, we suggest following sequences of events have resulted the bioherm development in Lower Cretaceous of Mongolia. First, simultaneous accumulation of abandoned caddisfly case aggregations and various growth forms of microbialites have formed irregular frameworks with high baffling capacity (Fig. 13C: Stage 1). Alternatively, it is possible that the decaying caddisfly cases provided stable growth sites hospitable for the microbialites (Fig. 12B,H). The silken threads of the caddisfly cases are rich in protein, which provided nutrients to benthic microorganisms. According to Stewart and others (2010), the caddisfly silk is made out of a protein named fibroin that contains a high amount of carbon and phosphorus. The paleoenvironment that these framework-building organisms inhabit was rich in various types of detrital grains, which resulted in a complex architecture of the

caddisfly cases. Second, these caddisfly/microbialite frameworks have trapped various types of skeletal and non-skeletal intraclasts including plant fragments, ooids, ostracod valves, and rare clastic grains. These intraclasts are seen as allochems in the thin sections (Fig. 10, 13C: Stage 2). Third, the open pore spaces between the caddisfly case/microbialite frameworks and trapped grains are packed with micrite dominated matrices (Fig. 10E,F, 11H, 13C: Stage 3). Concurrently, the remaining pore spaces are filled with the various types of syndepositional to early diagenetic cements in a short span of time. These cements likely precipitated from the carbonate rich lake waters (Fig. 10, 12, 13C: Stage 3). At last, the dissolution processes have occurred in the bioherm due to changes in the environment. The secondary vugular porosities have developed during this event, and are filled by late diagenetic cements during the meteoric diagenesis (Fig. 12B,L,M, 13C: Stage 4; Choquette et al., 1970; Flügel, 2010).

Based on these interpretations, we argue that the repeated accumulations of the caddisfly/microbialite frameworks and their baffled/trapped grains, as well as the matrices and generations of cements, altogether increased the volume of the carbonate deposition and resulted in bioherms with heterogeneous characteristics both spatially and temporally (Fig. 13B).

Paleoenvironment reconstruction

To reconstruct paleoenvironments, we focus on three main concepts: depositional setting (carbonate factory), lake water chemistry, and the lake basin dynamics. Depositional setting interpretations are largely based on fossil caddisfly case architecture analysis and overall bioherm composition. Lake chemistry interpretation depends on the

composition of the main bioherm components: matrices and cements. Based on the stratigraphic expression of the basin fill, we interpret changes in lake dynamics of the Tsagaansuvarga Basin over time.

Depositional setting. Caddisfly larvae and pupae capture a snapshot of their habitat by incorporating into their cases the most abundant materials available in their surrounding environment. Their cases reflect the composition of their habitat. Robust geological and paleontological analyses from the Eocene Green River Formation and other younger examples have successfully used caddisfly case architecture analysis for the paleoenvironment reconstructions (i.e., Loewen et al., 1999; Leggitt et al., 2001; 2007). The microbial-caddisfly bioherms of the Shinekhudag Formation are some of the oldest examples of fossil caddisfly cases (Lower Cretaceous age) and record involvement of the caddisfly larvae/pupae, in contrast to younger examples. Notably, these caddisflies are the first documented to have used plant fragments as case building material.

The following bioherm characteristics clarify complexities of their developmental setting. First, the coevolution of caddisfly cases and microbialites reveal a nutrient-rich, well-oxygenated environment, perhaps the littoral/photic zone of the lake with sufficient light for photosynthesis by the benthic microbial communities (Fig. 11, 12; Riding, 2000; Bohacs et al., 2007). Second, the abundant oolitic intraclasts and perfect spherical oncoidal fabrics suggest a shallow dynamic lake setting, above wave base (Fig. 12G,I; Rosenberg et al., 2015). Third, the caddisfly larvae/pupae introduced a large volume of detrital particles during bioherm development via building their cases with woody plant fragments (Fig. 11A,B,D,G,H). These plant armories reveal the immediate composition of the paleoenvironment; they are likely derived from in-situ trees growing along the lake

paleoshoreline (Keddy et al., 1986).

Based on these key features, we interpret the microbial-caddisfly bioherms as the lacustrine carbonate shoreline facies, deposited potentially in a carbonate-ramp setting with variable littoral energy (Platt & Wright, 1991; Wright, 2012). The subtle geometry of the ramp setting provided aggregation sites for caddisfly cases to build a framework (Fig. 14). Overall, our interpretation of Shinekhudag Formation bioherms agrees with key interpretations of the Green River Formation bioherms (Loewen et al., 1999; Leggitt et al., 2001; 2007; Buchheim et al., 2009; Seard et al., 2013; Awramik et al., 2015). Their similar framework-supported, mound-shaped carbonate facies with closely associated biological components (caddisfly larvae/pupae and microbial communities) strongly suggest that they were developed in analogous carbonate factories (Smith et al., 2008; Wright, 2012).

Lake chemistry. The carbonate-dominated matrices and syndepositional to early diagenetic cements (e.g., isopachous & fibrous calcite cements) of the bioherms reveal details of the lake chemistry (Fig. 10, 11, 12). The fine micrite matrices and calcitic cements precipitated in alkaline water rich in Ca/Mg and bicarbonate-ions (Fig. 10, 11, 12; Folk, 1974; Folk & Land, 1975). Additionally, a photosynthetic uptake of CO2 and/or bicarbonate of the filamentous cyanobacteria and algal mats potentially increased the lake alkalinity locally, thus enhancing the precipitation of carbonates (Burne et al., 1987; Riding, 2000). The abundant Ca/Mg ions are derived by erosion of the carbonate mineral-bearing basement, via surface water input from the surrounding hinterland, or Ca-rich spring waters (Shapley et al., 2005; Renaut & Gierlowski-Kordesch, 2010). However, we have not observed large faults near the microbial-caddisfly bioherm outcrops or tufa

fabrics that indicate local spring water discharge.

The lake water also might have contained sulfates, based on microscopic-scale gypsum crystals found from the bioherm pore spaces (Fig. 12J,K). In general, the evaporitic minerals in the lacustrine systems are indicative of saline-hypersaline lake water, often a result from the closed basin hydrology (Eugster et al., 1980; Carroll & Bohacs, 1999; 2001). Here, the saline-hypersaline lake condition may explain dolomite-dominated mineral composition of the micrite matrices and syndepositional to early diagenetic cements of the bioherms. This idea of early dolomitization is debatable, due to the limited extent of evaporitic minerals in the Tsagaansuvarga Basin as well as the general controversy regarding dolomite formation (Folk & Land, 1975; Warren, 2000). However, it could explain our results, and it requires further attention. In summary, we interpret that the paleo-lake chemistry was saline to hypersaline, rich Ca/Mg as well as biocarbonate ions, and relatively alkaline during the microbial-caddisfly bioherm deposition.

Lake dynamics. A close look at the microbial-caddisfly bioherms and the surrounding facies of the Shinekhudag Formation reveals a dynamic lake setting (Fig. 4B,C). The microbial-caddisfly bioherms are found within the lower interval (1800-2862 m) of the Shinekhudag Formation. The microbial-caddisfly bioherms are encased in a thick and discrete interval of oil-shale, interpreted as a classic distal lake deposit (Fig. 4C,5A,B,6); Powell, 1986; Fleet et al., 1988; Carroll and Bohacs, 2001). We interpret the lower interval as deposited in a balance-filled basin type, during a regional high-stand of the lake (Fig. 14). In contrast, our interpretations of depositional model as well as the paleoenvironment reconstruction both conclude the micbobial-caddisfly bioherms are a

littoral, nearshore lacustrine facies, deposited along the paleo lake shoreline (Platt & Wright, 1991; Wright, 2012).

This surprising stratigraphic juxtaposition is unique, compared to the analogous settings, especially when the linear biohermal (~1 km along strike) belt accumulated without disrupting the oil-shale accumulation (Fig. 2,6A,B,C). This oil-shale interval is significant, as it suggests that the stratified, anoxic bottom was not disturbed during the bioherm development (Fig. 14). Thus, we suggest that the microbial-caddisfly bioherms were deposited during a brief, rapid regression of a shrinking lake. Materials incorporated in the caddisfly case armories support this interpretation by revealing low pulses of clastic grains with rare biotites and feldspars that are likely derived from syndepositional volcanism (Fig. 11E,G). This building material selection may not be coincidental, especially if the lake hydrology was closed. Compared to the lacustrine microbialite facies-model of the Eocene Green River Formation, this theory of the hypersaline lake condition is controversial (Buchheim et al., 2012). However, this is an entirely viable scenario that could explain results presented in this paper.

In summary, the interpretations presented above suggest rapidly changing lake basin dynamics, transitioning from a balance-filled to an underfilled lake basin type and back, in a short span of time (Fig. 14). This rapidly changing lake basin type could either be controlled by superimposed paleoclimatic fluctuation (increased evaporation), and/or tectonically driven rapid basin subsidence, resulting in increased accommodation (Carroll & Bohacs, 2000).

Caddisfly taxonomic identification

Detailed investigation of the fossil caddisfly cases of the microbial-caddisfly bioherms of the Shinekhudag Formation reveals earlier underwater behavior of the caddisfly larvae. In 1968, Russian entomologist Sukatsheva reported the first discovery of fossil caddisflies and their cases from the Berriasian and Aptian of Mongolia (Sukatsheva, 1968;2016; Ivanov & Sukatsheva, 2002). However, no fossil caddisflies or their cases were reported from the Shinekhudag Formation or the Tsagaansuvarga Basin prior to our study. Here, we propose family level taxonomic identification of a caddisfly based on case architecture, size, and geometry without the associated fossil larvae.

Generally, the caddisflies are classified as Insecta Trichoptera and further divided into three main suborders: cocoon-making caddisflies (Spicipalpiai), retreat-making caddisflies (Annulipalpia), and portable case-makers (Integripalpia). Each of these suborders' cases can be distinguished by their definitive structure (McCafferty, 1983).

We use the following six main characteristics of the Shinekhudag Formation fossil cases to help tentatively assign their maker's family. First, the caddisfly communities of the Shinekhudag Formation lived around the littoral zone of a lake (Fig. 14). Second, both types of caddisfly cases (e.g., straight and curved) have similar tube shapes that are perfect circles in a cross section (Fig. 9, 11). Third, their lengths range from 7 to 21 mm and their width ranges between 1.5 to 2.5 mm (Fig. 8). Fourth, the poorly aligned to unaligned case groups reveal caddisfly larvae/pupae non-stationary life mode (Fig. 13). Finally, the progressively increased case size trends of the caddisfly cases (Fig. 8) reveal a case-abandonment behavior (Lloyd, 1921). In the modern examples, the caddisfly larvae/pupae abandon their cases under number of conditions, including an

environmental stress, a predator threatening, or a failure of cases to meet their convenience (Merrill, 1969; Wiggins, 1998).

Both the first and third characteristics (symmetrical shaped tubular shaped cases that are perfect circles in cross section and non-stationary life mode) are enough to assign the cases to the suborder Integripalpia—the portable case makers (Fig. 15; Mackay & Wiggins, 1979; Leggitt et al., 2001). It is due to the fact that the proctective cases of the other two suborders of caddisflies (Spicipalpiai and Annulipalpia) have assymetric, oval-shapes in cross section resulting from their stationary life-mode (Wiggins, 2004). The suborder Integripalpia includes total 33 families, but only three (Leptoceridae, Limnephilidae, and Phryganeidae) are adapted to the littoral lake zone, and build cylindrical tube shaped portable cases with detrital plant and rock fragments (Fig. 15; Wiggins, 2004; Holzenthal et al., 2007).

The earliest insect fossils and cases of the Leptoceridae and Phryganeidae are dated to early Cretaceous time, but the Limnephilidae appears in the fossil record much later, from the Oligocene (Fig. 15; Sukatsheva, 1968; Wiggins, 2015). Thus, we focus on the Leptoceridae and Phryganeidae families for the tentative assignment. Unfortunately, distinguishing between these two families based on their case morphology is challenging, and interestingly, these two families both occasionally show case-abandonment behavior during their larval/pupal stages (Lloyd, 1921; Wiggins, 1998). The only difference between these two families is the detailed architecture of their case construction. The modern family of the Phryganeidae builds neatly constructed, organized cases by using approximately even-sized, homogeneous types of armories. In contrast, the Leptoceridae build randomly constructed cases by using various-sized, heterogeneous types of

armories (Wiggins, 1998; 2004; Hinchliffe et al., 2010).

Overall, based on our observation, the caddisfly cases of the Shinekhudag Formation are composed of plainly constructed cases with various-sized, heterogeneous armors by using the most immediate materials from the surrounding environment (Fig. 9). Therefore, we conclude that the caddisfly cases of the Shinekhudag Formation are probably built by the family of Leptoceridae, analogous to the Early Cretaceous age South Korean caddisfly cases (Paik, 2005).

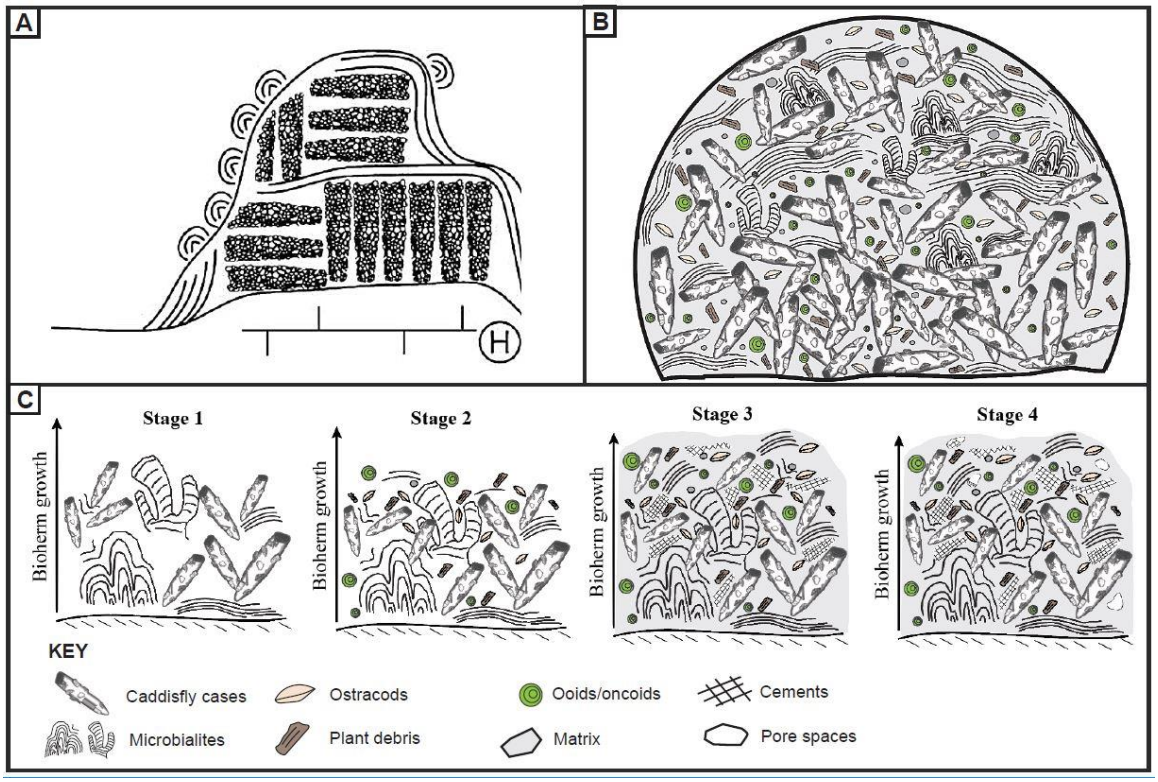

Figure 13. Development model of the microbial-caddisfly bioherms. (A) Development model of the Eocene Green River Formation (modified after Leggitt et al., 2001). (B) Development model of the Cretaceous Shinekhudag Formation. (C) Sequences of events that have resulted microbial-caddisfly bioherms of the Shinekhudag Formation. Please refer to the keys for diagram symbols.

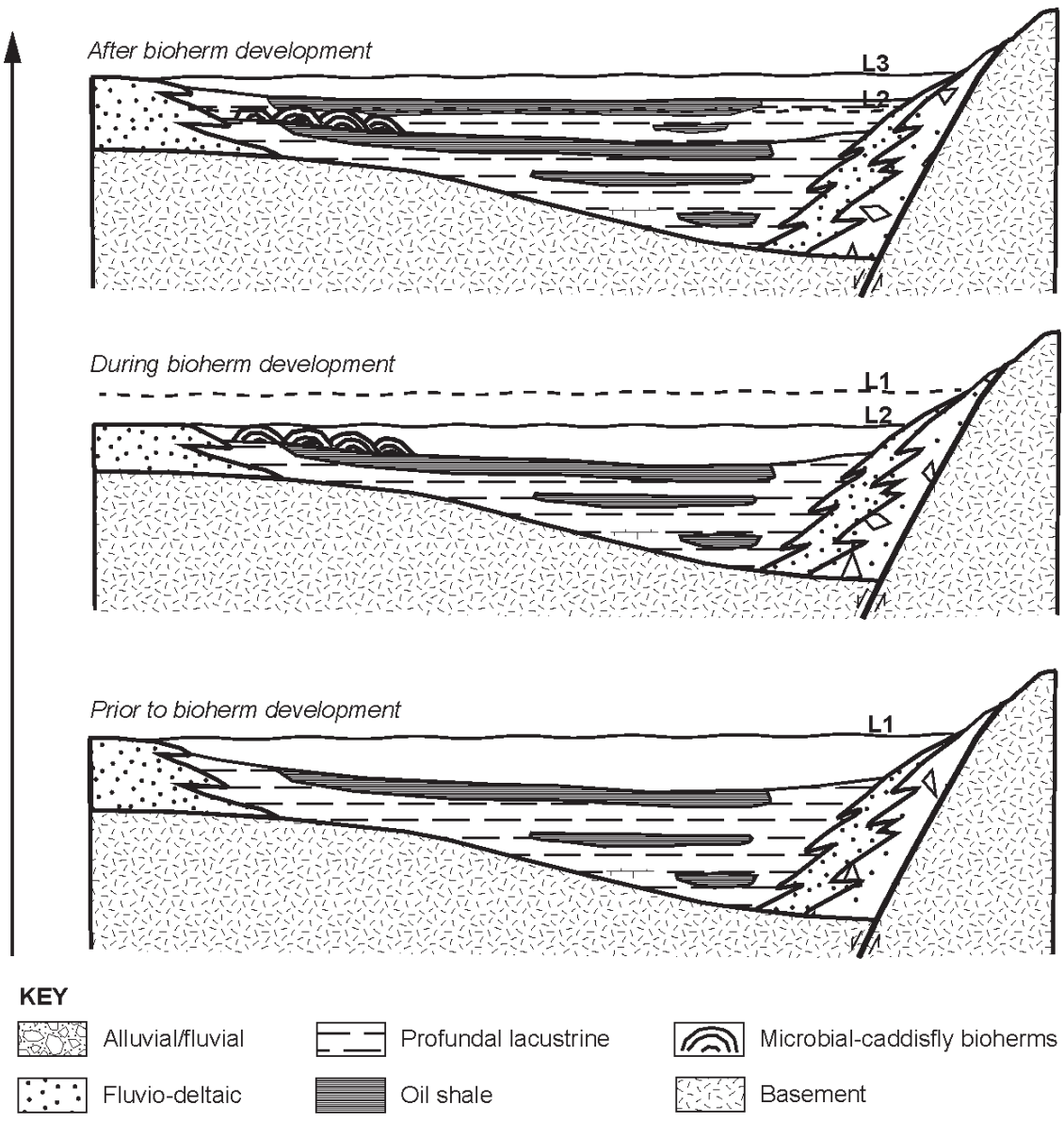

Figure 14. Schematic cross section of lake dynamics and associated facies. Please refer to the keys for diagram symbols.

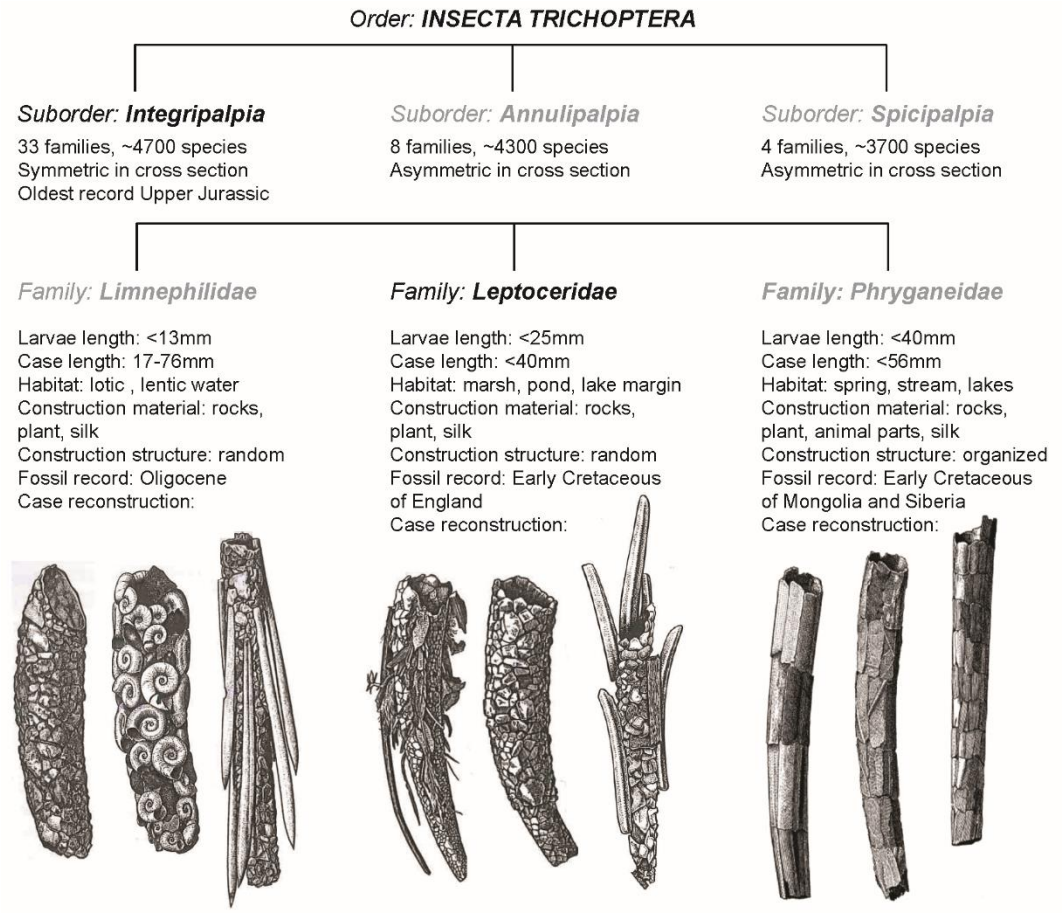

Figure 15 Caddisfly suborders and families (modified after Wiggins, 2004 and Holzenthal et al., 2007).

CONCLUSION

The first detailed description of the microbial-caddisfly bioherms of the Shinekhudag Formation reveals important aspects about lacustrine paleoenvironments during the late Mesozoic of southwestern Mongolia. A combination of the depositional environment interpretation of the basin fill, the development model of microbial-caddisfly bioherms, and the caddisfly case architecture analysis indicates a period of unstable lake condition—highly dynamic basin setting. Additionally, the architectural analysis of caddisfly cases contributes to an ancestral knowledge of caddisfly underwater behavior and demonstrates that caddisflies are important environmental indicators.

The Lower Cretaceous age microbial-caddisfly bioherms of the Shinekhudag Formation are one of the earliest examples documented globally. These bioherms are developed as a result of caddisfly case-microbialite dominated frameworks and their baffled/trapped grains, as well as matrices and cements that packed/cemented them together. The main bioherm building components (i.e., microbialites, caddisfly cases, cements, and matrices) suggest relatively alkaline, saline lake water that was rich in Ca/Mg and bicarbonate ions. It is also possible the lake water salinity was increased periodically to a hypersaline condition based on the early dolomitization process as well as the presence of minor gypsum cements that are inferred from the thin sections. The linear (~1 km) biohermal belt was developed along the lake paleolake shoreline, within a littoral zone. Based on the stratigraphic relationship of the bioherms as well as the

encasing oil-shale intervals, we argue the microbial-caddisfly bioherms were developed in a rapidly shrinking lake, a result of the lost balance of accommodation space and sediment+water supply.

Additionally, the caddisfly case architecture analysis reveals the interesting facts about lacustrine paleoenvironments. The fossil cases of caddisflies belong to a single species of the caddisfly larvae based on their case morphology. The plant materials, particularly wood pieces found from the caddisfly cases, represent the oldest record of fossil plant armor for caddisflies, and are derived from lake shoreline vegetation. Also, a few biotite and feldspar grains that are found from their cases suggest syndepositional magmatism. Arguably, the construction material selection of caddisfly larvae/pupae is mainly a factor of an availability of the detrital grains from their surrounding environment. Thus, it supports our interpretation of a lake basin with closed hydrology during the bioherm development. Without the associated fossil larvae/pupae, we tentatively attribute these fossil cases to the caddisfly family of Leptoceradae, a species that are previously known from the early Cretaceous lacustrine system of Korea (Paik, 2005).

APPENDIX A

CADDISFLY CASE SIZE MEASUREMENTS

A total of 115 caddisfly cases were measured from their caudal to cephalic ends on the hand sample eroded as well as polished surfaces. The measured caddisfly case sizes are provided in the Table 1. The hand samples are collected from the microbial-caddisfly bioherms of the Shinekhudag Formation of Mongolia. The sample locations are shown on Figure 2. The size measurements provided in Table 1 are the raw data for Figure 8.

Table 1. Caddisfly case size measurements

Caddisfly types	Length (mm)	Diameter (mm)
Straight	11.0	2.0
Straight	9.0	1.5
Straight	9.0	1.5
Straight	12.0	2.1
Straight	10.0	1.8
Straight	12.0	2.1
Straight	8.0	2.2
Straight	11.0	2.0
Straight	11.0	2.0
Straight	10.0	1.8
Straight	11.0	2.0
Straight	12.0	2.1
Straight	12.0	2.0
Straight	12.0	2.1
Straight	12.0	2.1
Straight	12.5	2.1
Straight	14.0	2.2
Straight	10.0	2.0
Straight	12.0	2.0
Straight	10.0	1.8
Straight	10.0	2.0
Straight	11.0	2.0
Straight	12.0	1.8

Caddisfly types	Length (mm)	Diameter (mm)
Straight	10.0	2.1
Straight	13.0	2.0
Straight	8.0	1.7
Straight	9.0	1.8
Straight	9.0	1.6
Straight	9.0	1.7
Straight	10.0	1.6
Straight	12.0	2.0
Straight	7.0	1.7
Straight	12.0	1.7
Straight	11.0	1.7
Straight	10.0	1.5
Straight	11.0	1.7
Straight	9.0	1.5
Straight	11.0	2.0
Straight	12.0	2.0
Straight	10.0	2.0
Straight	12.0	2.0
Straight	9.0	2.0
Straight	9.0	1.5
Straight	8.0	2.0
Straight	11.0	2.0
Straight	9.0	2.0

Table 1 continued

Caddisfly types	Length (mm)	Diameter (mm)
Straight	9.0	2.0
Straight	13.0	2.0
Straight	8.0	1.5
Straight	10.0	2.0
Straight	10.0	2.0
Straight	13.0	2.0
Straight	12.0	2.0
Straight	12.0	2.5
Straight	13.0	2.0
Straight	8.0	1.5
Straight	11.0	2.0
Straight	9.0	1.7
Straight	10.0	2.0
Straight	10.0	2.0
Straight	13.0	2.1
Straight	9.0	2.0
Straight	9.0	2.0
Straight	13.0	2.5
Straight	9.0	2.0
Straight	9.0	2.1
Straight	11.0	2.0
Straight	8.0	1.5
Straight	11.0	2.0
Straight	13.0	2.1
Straight	17.0	2.5

Caddisfly types	Length (mm)	Diameter (mm)
Straight	16.0	2.1
Straight	17.0	2.3
Straight	17.0	2.2
Straight	17.0	2.5
Straight	17.0	2.0
Straight	17.5	2.0
Straight	16.0	2.0
Straight	15.0	2.5
Straight	15.0	2.5
Straight	15.0	2.5
Straight	18.0	2.3
Straight	17.0	2.3
Straight	17.0	2.3
Straight	18.0	2.5
Straight	16.0	2.0
Straight	17.0	2.5
Straight	17.0	2.1
Straight	15.0	2.5
Straight	17.0	2.5
Straight	21.0	2.5
Straight	16.0	2.1
Straight	17.0	2.2
Straight	18.0	2.5
Straight	19.0	2.5
Straight	17.5	2.5

Table 1 continued

Caddisfly types	Length (mm)	Diameter (mm)
Straight	17.0	2.5
Straight	16.0	2.5
Straight	18.0	2.5
Straight	18.0	2.0
Straight	17.0	2.0
Straight	19.0	2.5
Straight	16.0	2.0
Curved	10.0	2.0
Curved	11.0	2.1
Curved	12.0	2.0
Curved	9.0	1.5
Curved	10.0	2.0
Curved	10.5	2.0
Curved	8.0	2.0
Curved	12.0	2.0
Curved	12.0	2.1
Curved	12.0	2.0
Curved	11.0	1.8
Curved	12.0	1.7

APPENDIX B

CADDISLFY CASE ARMOR CLAST COUNTS AND SIZES

A total of 160 clasts were counted from the caddisfly cases in thin section for caddisfly case architecture analysis. The measured caddisfly armor sizes are provided in Table 2. The average clast percentage and sizes are discussed in the text under the BIOHERM ANALYSIS.

Table 2. Caddisfly case armor clast counts and sizes

Clast type	Length (mm)	Width (mm)
Ostracod	0.46	0.02
Ostracod	0.41	0.01
Ostracod	0.32	0.02
Ostracod	0.59	0.12
Ostracod	0.33	0.02
Ostracod	0.34	0.02
Ostracod	0.45	0.02
Ostracod	0.67	0.02
Ostracod	0.96	0.03
Ostracod	0.74	0.03
Ostracod	0.44	0.02
Ostracod	0.92	0.03
Ostracod	0.35	0.02
Ostracod	0.42	0.02
Ostracod	0.7	0.06
Ostracod	0.48	0.04
Ostracod	0.28	0.02
Ostracod	0.53	0.02
Ostracod	0.57	0.02
Ostracod	0.53	0.04
Ostracod	0.43	0.03
Ostracod	0.77	0.23
Ostracod	0.29	0.01

Clast type	Length (mm)	Width (mm)
Ostracod	0.26	0.01
Ostracod	0.87	0.22
Ostracod	0.81	0.05
Ostracod	1.14	0.14
Ostracod	1.15	0.35
Ostracod	0.52	0.06
Ostracod	0.75	0.06
Plant material	0.31	0.03
Plant material	0.25	0.08
Plant material	0.29	0.09
Plant material	0.74	0.23
Plant material	0.37	0.32
Plant material	1.08	0.36
Plant material	0.74	0.25
Plant material	0.72	0.1
Plant material	0.24	0.05
Plant material	0.25	0.08
Plant material	0.53	0.07
Plant material	0.58	0.15
Plant material	0.59	0.02
Plant material	0.97	0.02
Plant material	0.24	0.02
Plant material	0.51	0.22

Table 2 continued

Clast type	Length (mm)	Width (mm)
Plant material	0.39	0.13
Plant material	0.4	0.1
Plant material	0.18	0.02
Plant material	0.23	0.02
Plant material	1.33	0.14
Plant material	0.8	0.11
Plant material	0.54	0.08
Plant material	1.15	0.21
Plant material	0.57	0.08
Plant material	0.64	0.17
Plant material	0.37	0.1
Plant material	0.9	0.43
Plant material	0.92	0.24
Plant material	0.74	0.15
Plant material	1.04	0.03
Plant material	0.82	0.07
Plant material	0.65	0.12
Plant material	0.65	0.06
Plant material	0.66	0.09
Plant material	0.78	0.11
Plant material	0.91	0.17
Plant material	0.84	0.1
Plant material	0.93	0.1
Plant material	0.65	0.1
Plant material	0.61	0.1

Clast type	Length (mm)	Width (mm)
Plant material	0.58	0.08
Plant material	0.7	0.1
Plant material	0.59	0.13
Plant material	0.52	0.08
Plant material	0.55	0.07
Plant material	0.48	0.07
Plant material	0.53	0.11
Plant material	0.89	0.13
Plant material	0.54	0.08
Plant material	0.42	0.04
Plant material	1.97	0.32
Plant material	1.06	0.29
Plant material	0.62	0.07
Plant material	0.66	0.09
Plant material	0.62	0.1
Plant material	0.82	0.08
Plant material	0.73	0.03
Plant material	0.85	0.03
Plant material	1.95	0.2
Plant material	0.64	0.53
Plant material	0.77	0.1
Plant material	0.53	0.21
Plant material	0.43	0.07
Plant material	0.37	0.08
Plant material	0.43	0.28

Table 2 continued

Clast type	Length (mm)	Width (mm)
Plant material	0.85	0.07
Plant material	0.8	0.11
Plant material	0.58	0.04
Plant material	0.58	0.07
Plant material	0.36	0.18
Plant material	0.2	0.12
Plant material	0.48	0.08
Plant material	0.76	0.07
Plant material	0.35	0.21
Plant material	0.56	0.08
Plant material	0.32	0.04
Plant material	0.77	0.04
Plant material	0.65	0.05
Plant material	0.35	0.02
Plant material	0.33	0.01
Plant material	0.44	0.02
Plant material	0.56	0.03
Plant material	0.45	0.03
Plant material	0.42	0.03
Plant material	1.67	0.34
Plant material	0.68	0.12
Plant material	0.53	0.06
Plant material	0.84	0.06
Plant material	0.73	0.04
Plant material	0.93	0.04
Plant material	0.96	0.05
Plant material	1.07	0.09
Plant material	0.8	0.09
Plant material	0.72	0.05
Plant material	0.53	0.03
Plant material	0.71	0.16
Plant material	0.41	0.08
Plant material	0.25	0.11
Plant material	0.44	0.02
Plant material	0.02	0.1
Plant material	0.52	0.03
Plant material	0.88	0.04
Plant material	0.81	0.14
Plant material	0.68	0.02
Plant material	0.69	0.04
Plant material	0.69	0.09
Plant material	1.97	0.53
Feldspar	0.7	0.34
Feldspar	0.63	0.35
Feldspar	0.29	0.15
Feldspar	0.17	0.12
Feldspar	0.33	0.17
Feldspar	0.37	0.22
Biotite	0.2	0.04
Biotite	0.2	0.04

Table 2 continued

Clast type	Length (mm)	Width (mm)
Biotite	0.3	0.05
Biotite	0.3	0.03
Biotite	0.27	0.04
Biotite	0.15	0.03
Biotite	0.3	0.02
Biotite	0.26	0.03
Biotite	0.3	0.03
Biotite	0.33	0.03
Biotite	0.2	0.04
Biotite	0.37	0.07
CRF	0.77	0.33
CRF	0.61	0.3
CRF	0.31	0.2
CRF	0.28	0.14

REFERENCES

Ali S.A, Clark W.J, Moore W.R, Dribus J.R, 2010, Diagenesis and reservoir quality: Oilfield Review, v. 22, p. 14-27.

Ariunchimeg Y, Badamgarav D, Byamba J, Dorjnamjaa D, Makhbadar, T, Minjin C, Narantsetseg Ts, Orolmaa D, Sersmaa G, 2012, Geology and Mineral Resources of Mongolia, Chapter 8: Ulaanbaatar, Mongolia, p. 408-496.

Awramik S.M, Buchheim H.P, 2015, Giant stromatolites of the Eocene Green River Formation (Colorado, USA): Geology, v. 43, p. 691-694.

Badarch G, Cunningham W.D, Windley B.F, 2002, A new terrane subdivision for Mongolia: implications for the Phanerozoic crustal growth of Central Asia: Journal of Asian Earth Sciences, v. 21, p. 87-110.

Baskin R.L, 2014, Occurrence and spatial distribution of microbial bioherms in Great Salt Lake, Utah: Salt Lake City, The University of Utah.

Bhattacharya J.P, 2006, Deltas: Special Publication-SEPM, v. 84, p. 237.

Bohacs K.M, Carroll A.R, Neal J.E, Mankiewicz P.J, 2000, Lake-basin type, source potential, and hydrocarbon character: an integrated sequence-stratigraphic-geochemical framework. Lake basins through space and time: AAPG Studies in Geology, v. 46, p. 3-4.

Bohacs K.M, Hasiotis S.T, Demko T.M, 2007, Continental ichnofossils of the Green River and Wasatch Formations, Eocene, Wyoming: a preliminary survey, proposed relation to lake-basin type, and application to integrated paleo-environmental interpretation: AAPG Bulletin, v. 44, p, 79-108.

Botosaneanu L, Giudicelli J, 2004, Contributions to the knowledge of the fauna of caddisflies (Insecta: Trichoptera) from south-east France, with description of new taxa: InAnnales de Limnologie-International Journal of Limnology, v. 40, p. 15-32.

Braithwaite C.J, 1991, Dolomites, a review of origins, geometry and textures: Earth Sciences, v. 82, p. 99-112.

Bridge J.S, 1991, Description and interpretation of fluvial deposits: a critical perspective: Sedimentology, v. 40, p. 801-810.

Buchheim H.P, Awramik S.M, Leggitt V.L, Demko T.M, Lamb-Wozniak K, Bohacs K.M, 2012, Large lacustrine microbialite bioherms from the Eocene Green River Formation: stratigraphic architecture, sequence stratigraphic relations, and depositional model: In AAPG Hedberg Conference, Microbial Carbonate Reservoir Characterization Abstracts, American Association of Petroleum Geologists, Tulsa, OK

Buchheim H.P, Awramik S.M, Leggitt V.L, 2009, Paleoenvironmental factors controlling microbialite bioherm deposition and distribution in the Green River Formation: In 2009 Portland GSA Annual Meeting.

Bull W.B, 1972, Recognition of alluvial fan deposits in stratigraphic record. In: Recognition of Ancient Sedimentary Environments: Society of Economic Paleontologists, Mineralogists Special Publication, v. 16, p. 63-83.

Burne R.V, Moore L.S, 1987, Microbialites: organosedimentary deposits of benthic microbial communities: Palaios, v. 2, p. 241-254.

Carroll A.R, Bohacs K.M, 1999, Stratigraphic classification of ancient lakes: Balancing tectonic and climatic controls: Geology, v. 27, p. 99-102.

Carroll A.R, Bohacs K.M, 2001, Lake-type controls on petroleum source rock potential in nonmarine basins: AAPG bulletin, v. 85, p. 1033-1053.

Chafetz H.S, 2013, Porosity in bacterially induced carbonates: Focus on micropores: AAPG bulletin, v. 97, p. 2103-2111.

Choquette P.W, Pray L.C, 1970, Geologic nomenclature and classification of porosity in sedimentary carbonates: AAPG bulletin, v. 54, p. 207-250.

Cohen A.S, 1989, Facies relationships and sedimentation in large rift lakes and implications for hydrocarbon exploration: examples from Lakes Turkana and Tanganyika: Palaeogeography, Palaeoclimatology, Palaeoecology, v. 70, p. 65-80.

Coleman J.M, Prior D.B, 1982, Deltaic environments of deposition: AAPG Special Volumes, p. 139-178.

Cunningham D, 2005, Active intracontinental transpressional mountain building in the Mongolian Altai: defining a new class of orogeny: Earth and Planetary Science Letters, v. 240, p. 436-444.

Cunningham D, 2010, Tectonic setting and structural evolution of the Late Cenozoic Gobi Altai orogeny: Geological Society, London, Special Publications, v. 338, p. 361-387.

Dickson J.A, 1966, Carbonate identification and genesis as revealed by staining: Journal of Sedimentary Research, v. 36, p. 491-505.

Drysdale R.N, Carthew K.D, Taylor M.P, 2003, Larval caddis-fly nets and retreats: a unique biosedimentary paleocurrent indicator for fossil tufa deposits: Sedimentary Geology, v. 161, p. 207-215.

Dumitru T.A, Hendrix M.S, 2001, Fission-track constraints on Jurassic folding and thrusting in southern Mongolia and their relationship to the Beishan thrust belt of northern China: MEMOIRS-GEOLOGICAL SOCIETY OF AMERICA, p. 215-230.

Dunham R.J, 1962, Classification of carbonate rocks according to depositional textures: American Association of Petroleum Geologists Memoir, v. 1, p. 108–121.

Dupraz C, Visscher P.T, Baumgartner L.K, Reid R.P, 2004, Microbe–mineral interactions: early carbonate precipitation in a hypersaline lake (Eleuthera Island, Bahamas): Sedimentology, v. 51, p. 745-765.

Elias S.A, 1991, Insects and climate change: Bioscience, v. 41, p. 552-559.

Embry III A.F, Klovan J.E, 1971, A late Devonian reef tract on northeastern Banks Island, NWT: Bulletin of Canadian Petroleum Geology, v. 19, p. 730-781.

Eugster H.P, Kelts K, 1983, Lacustrine chemical sediments. Chemical Sediments and Geomorphology: London, Academic Press, p. 321-368.

Fleet A.J, Kelts K, Talbot M, 1988, Lacustrine petroleum source rocks: Geological Society Special Publication, v. 40.

Flügel E, 1982, Sedimentation RC. Microfacies analysis of limestones: Berlin, Springer-Verlag Berlin Heidelberg

Flügel E, 2010, Microfacies of Carbonate Rocks, 2nd edition: Berlin, Springer-Verlag Berlin Heidelberg.

Flügel E, 2004, Microfacies Data: Fabrics In Microfacies of Carbonate Rocks: Berlin, Springer-Verlag, p. 177-242.

Folk R.L, 1974, The natural history of crystalline calcium carbonate: effect of magnesium content and salinity: Journal of Sedimentary Research, v. 44, p. 40-53.

Folk R.L, Land L.S, 1975, Mg/Ca ratio and salinity: two controls over crystallization of dolomite: AAPG bulletin, v. 59, p. 60-68.

Frantz C.M, 2013, Stromatolites as biosignatures and paleoenvironmental records: experiments with modern mats and examples from the Eocene Green River Format: Los Angeles, University of Southern California.

Frantz C.M, Petryshyn V.A, Corsetti F.A, 2015, Grain trapping by filamentous cyanobacterial and algal mats: implications for stromatolite microfabrics through time: Geobiology, v. 13, p. 409-423.

Friedman G.M, 1959, Identification of carbonate minerals by staining methods: Journal of Sedimentary Research, v. 29, p. 87-97.

Graham S.A, Cope T, Johnson C.L, Ritts B, 2012, Sedimentary basins of the late Mesozoic extensional domain of China and Mongolia in Regional geology and tectonics: Phanerozoic rift systems and sedimentary basins, Volume 2: Amsterdam, Netherlads, Elsevier, p. 442-461, doi: 10.1016/B978-0-444-56356-9.00016-X.

Hinchliffe R, Palmer A.R, 2010, Curious chiral cases of caddisfly larvae: handed behavior, asymmetric forms, evolutionary history: Integrative and comparative biology, v. 50, p. 606-618.

Holzenthal R.W, Blahnik R.J, Prather A.L, Kjer K.M, 2007, Order Trichoptera Kirby, 1813 (Insecta), Caddisflies: Zootaxa, v. 1668, p. 639-698.

Horton B.K, Constenius K, Tully J, Coogan J, Menotti T, Davaa B et al., 2013, Late Jurassic Early Cretaceous synrift sedimentation in Tsagaansuvarga Basin of Gobi Altai region of SW Mongolia: In AAPG Annual Convention and Exhibition, AAPG Search and Discovery, Long Beach, v. 10487.

Hugueney M.A, Tachet H.E, Escuillié F.R, 1990, Caddisfly pupae from the Miocene indusial limestone of Saint-Gérand-le-Puy, France: Palaeontology, v. 33, p. 495-502.

Ivanov V.D, Sukatsheva I.D, 2002, Trichoptera (Phryganeida). History of Insects: London, Kluwer Academic Publishers, p. 199-220.

Johnson C.L, Webb L.E, Graham S.A, Hendrix M.S, Badarch G, 2001, Sedimentary and structural records of late Mesozoic high-strain extension

and strain partitioning, East Gobi basin, southern Mongolia: Memoirs-Geological Society of America, p. 413-434.

Johnson C.L, Greene T.J, Zinniker D.A, Moldowan J.M, Hendrix M.S, Carroll A.R, 2003, Geochemical characteristics and correlation of oil and nonmarine source rocks from Mongolia: AAPG bulletin, v. 87, p. 817-846.

Johnson C.L, 2004, Polyphase evolution of the East Gobi basin: sedimentary and structural records of Mesozoic–Cenozoic intraplate deformation in Mongolia: Basin Research, v. 16, p. 79-99.

Johnson C.L, Constenius K.C, Graham S.A, Mackey G, Menotti T, Payton A, Tully J, 2015, Subsurface evidence for late Mesozoic extension in western Mongolia: Tectonic and petroleum systems implications: Basin Research, v. 27, p. 272-294.

Keddy P.A, Reznicek A.A, 1986, Great Lakes vegetation dynamics: the role of fluctuating water levels and buried seeds: Journal of Great Lakes Research, v. 12, p. 25-36.

Keller A.M, Hendrix M.S, 1997, Paleoclimatologic analysis of a Late Jurassic petrified forest, southeastern Mongolia: Palaios, v. 12, p. 282-291.

Kelts K, Hsü K.J, 1978, Freshwater carbonate sedimentation in Lakes: New York, Springer-Verlag, p. 295-323.

Kelty T.K, Yin A, Dash B, Gehrels G.E, Ribeiro A.E, 2008, Detrital-zircon geochronology of Paleozoic sedimentary rocks in the Hangay–Hentey basin, north-central Mongolia: implications for the tectonic evolution of the Mongol–Okhotsk Ocean in central Asia: Tectonophysics, v. 451, p. 290-311.

Klement K.W, 1967, Practical Classification of Reefs and Banks, Bioherms and Biostromes: AAPG Bulletin, v. 51, p. 167-168.

Kuzmina S, Elias S, Matheus P, Storer J.E, Sher A, 2008, Paleoenvironmental reconstruction of the Last Glacial Maximum, inferred from insect fossils from a tephra buried soil at Tempest Lake, Seward Peninsula, Alaska: Palaeogeography, Palaeoclimatology, Palaeoecology, v. 267, p. 245-255.

Leggitt V.L, Biaggi R.E, Buchheim H, 2007, Palaeoenvironments associated with caddisfly-dominated microbial-carbonate mounds from the Tipton Shale Member of the Green River Formation: Eocene Lake Gosiute: Sedimentology, v. 54, p. 661-699.

Leggitt V.L, Cushman R.A, 2001, Complex caddisfly-dominated bioherms from the Eocene Green River Formation: Sedimentary Geology, v. 145, v. 377-396.

Leggitt V.L, Loewen MA, 2002, Eocene Green River Formation “Oocardium tufa” reinterpreted as complex arrays of calcified caddisfly (Insecta: Trichoptera) larval cases: Sedimentary Geology, v. 148, p. 139-146.

Lloyd J.T, 1921, The Biology of North American Caddis Fly Larvae: Ithaca, New York, Cornell University.

Loewen M.A, Leggitt V.L, Buchheim H.P, 1999, Caddisfly (Trichoptera) larval cases from Eocene Fossil Lake, Fossil Butte National Monument: National Park Service Paleontological Research, p. 72-77.

Mackay R.J, Wiggins G.B, 1979, Ecological diversity in Trichoptera: Annual Review of Entomology, v. 24, p. 185-208.

Mancini E.A, Morgan W.A, Harris P.M, Parcell W.C, 2013, Microbial Carbonate Reservoir Characterization—Conference summary and selected papers: AAPG Bulletin, v. 97, p. 1835-1847.

McCafferty W.P, 1983, Aquatic entomology: the fishermen's and ecologists' illustrated guide to insects and their relatives: Toronto, Canada, Jones & Bartlett Publishers.

McPherson J.G, Shanmugam G, Moiola R.J, 1987, Fan-deltas and braid deltas: Varieties of coarse-grained deltas: Geological Society of America Bulletin, v. 99, p. 331-340.

Meadows A, Meadows P.S, Wood D.M, Murray J.M, 1994, Microbiological effects on slope stability: an experimental analysis: Sedimentology, v. 41, p. 423-435.

Meng Q.R, 2003, What drove late Mesozoic extension of the northern China–Mongolia tract?: Tectonophysics, v. 369, p. 155-174.

Merrill D, 1969, The distribution of case recognition behaviour in ten families of caddis larvae (Trichoptera): Animal Behaviour, v. 17, p. 486-493.

Miall A.D, 1996, The geology of fluvial deposits. Sedimentary Facies, Basin Analysis, and Petroleum Geology: Berlin, Heidelberg, New York, London, Paris, Tokyo, Hong Kong, Springer-Verlag, 598 p.

Neal J.E, Bohacs K.M, Reynolds D.J, Scholz C.A, 1997, Sequence stratigraphy of lacustrine rift basins: Critical linkage of changing lake level, sediment supply, and tectonics: Geological Society of America Abstracts with Programs, v. 6, p. 239.

Nemec W, Steel RJ. What is a fan delta and how do we recognize it. Fan Deltas in Sedimentology and Tectonic Settings, p. 3-13.

Paik I.S, 2005, The oldest record of microbial-caddisfly bioherms from the Early Cretaceous Jinju Formation, Korea: occurrence and palaeoenvironmental implications: Palaeogeography, Palaeoclimatology, Palaeoecology, v. 218, p. 301-315.

Platt N.H, Wright V.P. 1991, Lacustrine Facies Analysis in Special Publication of IAS: John Wiley *& Sons, v. 30, 328 p.

Postma G, 1990, Depositional architecture and facies of river and fan deltas: a synthesis. Coarse-grained deltas: Special Publication in Association of Sedimentary Geologists, v. 10, p. 13-27.

Powell T.G, 1986, Petroleum geochemistry and depositional setting of lacustrine source rocks: Marine and Petroleum Geology, v. 3, p. 200-219.

Prost G.L, 2004, Tectonics and hydrocarbon systems of the East Gobi basin, Mongolia: AAPG bulletin, v. 88, p. 483-513.

Renaut R.W, Gierlowski-Kordesch EH, 2010, Lakes, Facies models, Noel, P.J, Dalrymple, R.W, Facies Model: Calgary, Canada, p. 541-575.

Riding R, 1991, Classification of microbial carbonates, Calcareous algae and stromatolites: Berlin, Springer-Verlag, doi: 10.1007/978-3-642-52335-9_2, p. 21-51.

Riding R, 2000, Microbial carbonates: the geological record of calcified bacterial–algal mats and biofilms: Sedimentology, v. 47, p. 179-214.

Rosenberg M.J, Birgenheier L.P, Berg M.D, 2015, Facies, stratigraphic architecture, and lake evolution of the oil shale bearing Green River Formation, eastern Uinta basin, Utah, Stratigraphy and Paleolimnology of the Green River Formation, Western USA: Netherlands, Springer-Verlag, p. 211-249.

Ross H.H, 1967, The evolution and past dispersal of the Trichoptera: Annual review of entomology, v. 12, p. 169-206.

Schieber J, Southard J.B, Kissling P, Rossman B, Ginsburg R, 2013, Experimental deposition of carbonate mud from moving suspensions: importance of flocculation and implications for modern and ancient carbonate mud deposition: Journal of Sedimentary Research, v. 83, p. 1025-1031.

Schnurrenberger D, Russell J, Kelts K, 2003, Classification of lacustrine sediments based on sedimentary components: Journal of Paleolimnology, v. 29, p. 141-154.

Scholle P.A, Ulmer-Scholle D.S, 2003, A Color Guide to the Petrography of Carbonate Rocks: Grains, Textures, Porosity, Diagenesis: AAPG Memoir, v. 77.

Seard C, Camoin G, Rouchy J.M, Virgone A, 2013, Composition, structure and evolution of a lacustrine carbonate margin dominated by microbialites: Case study from the Green River formation (Eocene; Wyoming, USA): Palaeogeography, Palaeoclimatology, Palaeoecology, v. 381, p. 128-144.

Semikhatov M.A, Gebelein C.D, Cloud P, Awramik S.M, Benmore W.C, 1979, Stromatolite morphogenesis-progress and problems: Canadian Journal of Earth Sciences, v. 16, p. 992-1015.

Shapiro R.S, 2000, A comment on the systematic confusion of thrombolites: Palaios, v. 15, p. 166-169.

Shapley M.D, Ito E, Donovan J.J, 2005, Authigenic calcium carbonate flux in groundwater-controlled lakes: implications for lacustrine paleoclimate records: Geochimica et Cosmochimica Acta, v. 69, p. 2517-2533.

Shcherbakov D.E, 2008, Insect recovery after the Permian/Triassic crisis: Alavesia, v. 2, p. 125-131.

Sibley D.F, Gregg J.M, 1987, Classification of dolomite rock textures: Journal of Sedimentary Research, v. 57, p. 967-975.

Sibley D.F, 1991, Secular changes in the amount and texture of dolomite: Geology, v. 19, p. 151-154.

Smith M.E, Carroll A.R, Singer B.S, 2008, Synoptic reconstruction of a major ancient lake system: Eocene Green River Formation, western United States: Geological Society of America Bulletin, v. 120, p. 54-84.

Statzner B, Dolédec S, 2011, Mineral grain availability and pupal-case building by lotic caddisflies: Effects on case architecture, stability and building

expenses: Limnologica-Ecology and Management of Inland Waters, v. 41, p. 266-280.

Stewart R.J, Wang C.S, 2010, Adaptation of caddisfly larval silks to aquatic habitats by phosphorylation of H-fibroin serines: Biomacromolecules, v. 11, p. 969-974.

Sukatsheva I.D, 2016, The family Phryganeidae (Insecta, Trichoptera) from the Mesozoic and Cenozoic of Asia (with a brief worldwide overview of the fossil caddisfly fauna): Paleontological Journal, v. 50, p. 369-405.

Sukatsheva I.D, 1968, The Mesozoic caddisflies (Trichoptera) from Transbaikalia: Paleontological Journal, v. 2, p. 59-75.

Tànavsuu-Milkeviciene K.A, Frederick Sarg J. 2012, Evolution of an organic-rich lake basin–stratigraphy, climate and tectonics: Piceance Creek basin, Eocene Green River Formation: Sedimentology, v. 59, p. 1735-1768.

Thompson J.B, Ferris F.G, 1990, Cyanobacterial precipitation of gypsum, calcite, and magnesite from natural alkaline lake water: Geology, v. 18, p. 995-998.

Traynor J.J, Sladen C. 1995, Tectonic and stratigraphic evolution of the Mongolian People's Republic and its influence on hydrocarbon geology and potential: Marine and Petroleum Geology, v. 12, p. 35-52.

Tully J., Barnwell A. 2015, Mongolia. Potential in an Emerging Economy: GeoExpro, v. 11, p. 48-52.

Vincent S.J, Allen M.B, 2001, Sedimentary record of Mesozoic intracontinental deformation in the eastern Junggar Basin, northwest China: response to orogeny at the Asian margin: Memoirs-Geological Society of America, p. 341-360.

Warren J, 2000, Dolomite: occurrence, evolution and economically important associations: Earth-Science Reviews, v. 52, p. 1-81.

Watson M.P, Hayward A.B, Parkinson D.N, Zhang Z.M, 1987, Plate tectonic history, basin development and petroleum source rock deposition onshore China: Marine and Petroleum Geology, v. 4, p. 205-225.

Webb L.E, Graham S.A, Johnson C.L, Badarch G, Hendrix M.S, 1999, Occurrence, age, and implications of the Yagan–Onch Hayrhan metamorphic core complex, southern Mongolia: Geology, v. 27, p. 143-1999 Feb 1;27(2):143-146.

Wells J.T, Scholz C.A, Soreghan M.J, 1999, Processes of sedimentation on a lacustrine border-fault margin: interpretation of cores from Lake Malawi, East Africa: Journal of Sedimentary Research, v. 69, p. 816-831.

Wiggins G.B, 1998, The caddisfly family Phryganeidae (Trichoptera): Toronto, University of Toronto Press

Wiggins G.B, 2004, Caddisflies: the underwater architects: Toronto, University of Toronto Press.

Wiggins G.B, 2015, Larvae of the North American caddisfly genera (Trichoptera): Toronto, University of Toronto Press.

Wilson M.V, 1980, Eocene lake environments: depth and distance-from-shore variation in fish, insect, and plant assemblages: Palaeogeography, Palaeoclimatology, Palaeoecology, v. 32, p. 21-44.

Wilson M.V, 1988, Reconstruction of ancient lake environments using both autochthonous and allochthonous fossils: Palaeogeography, Palaeoclimatology, Palaeoecology, v. 62, p. 609-623.

Wright V.P, 2012, Lacustrine carbonates in rift settings: the interaction of volcanic and microbial processes on carbonate deposition: Geological Society, London, Special Publications, v. 370, p. 39-47.

Zabotkin L, Misiondz, K, Dobrov, M, Bochkov, S, Nikitin, L, Vertlib, V, 1988, The result of the 1:200000 scale geological mapping of the Bayankhongor province, Mongolia, Report No 4276: Ulaanbaatar, Mongolia.

Zheng Y, Zhang Q, Wang Y, Liu R, Wang S.G, Zuo G, Wang S.Z, Lkaasuren B, Badarch G, Badamgarav Z, 1996, Great Jurassic thrust sheets in Beishan (North Mountains)—Gobi areas of China and southern Mongolia: Journal of Structural Geology, v. 18, p. 1111-1126.